# Identifying and Modeling Evaporite Facies using Well Logs: Characterising the Devonian Elk Point Group salt giant

by

Elaine Loretta Lord

A thesis submitted in partial fulfillment of the requirements for the degree of

Master of Science

Department of Earth and Atmospheric Sciences

University of Alberta

## Abstract

Over the last century, study of evaporite deposits has evolved from modeling chemical successions and studying outcrops of insoluble material, to sedimentologic study of drill core paired with geochemical analysis. In this thesis, I add to published scientific literature on the Prairie Evaporite Formation, a succession of Middle-Devonian evaporate deposits in the Central Alberta Basin of Alberta, Canada. I combine new well log interpretation with sedimentologic studies in the literature to define six new evaporite facies in the Prairie Evaporite Formation, and present a new facies identification scheme that correlates wireline log signatures to core log data. Wireline log data from 994 wells and logs of seven cores in the Central Alberta Basin are compiled to assess stratigraphic relationships, lithological facies, textural features, and insoluble marker beds within the Prairie Evaporite Formation. This analysis identifies seven unique facies sequences within each cycle of the Prairie Evaporite in the Central Alberta Basin. I have produced 3D-facies models for each cycle in order to map facies distribution across the Central Alberta Basin and assess the change in depositional environments through time and across the basin. I infer water cyclicity and climate in the basin during the middle Devonian based on these depositional environments: modeled facies reflect a nearshore environment in the west and southwest Central Alberta Basin and an increasingly shallow and concentrated epeiric sea basinward. I speculate that application of this facies correlation scheme to other evaporite deposits of the world is possible, but requires calibration by correlation of wireline log data to core log data.

## Acknowledgements

I would like to acknowledge my supervisor, Dr. Nicholas Harris, for being the inspiration of this project and the CAES program for giving me the opportunity to study at the University of Alberta. Thank you to Piotr Kukiolka, Chris Schneider, and Tim Lowenstein for exposing me to the fascinating and unique world of evaporites as well as for laying the groundwork of my knowledge. I would also like to thank Dr. Murray Gingras and Dr. Daniel Alessi for their help with sample analysis. Thank you to Mark and Walt for their assistance in any sample processing procedures, their time and dedication to creative problem solving is the reason that I was able to safely produce samples for analysis. Thank you to Konstantin Von Gunten and Guang Cheng for providing his time to produce ICP-MS data, and Katie Hogberg for her time spent towards XRD analysis. This project also could not have happened without the generous sample lending program from the AER-CRC and all of those who worked on these formations before me. I acknowledge the support of the Natural Sciences and Engineering Research Council of Canada (NSERC) through grant # CRDPJ 477323 – 14 and Alberta Innovates through grant #20150003336. I also acknowledge the financial support of Rocky Mountain Power (now Rocky Mountain Power Energy Storage) and the encouragement and support of Jan van Egteren and Robert Stewart. I thank Vermillion Energy, Newalta Corporation, and Esso for allowing me to sample cores under their care. I thank Maurice Dusseault and Sean McKenna of the University of Waterloo for engaging me in the broader topic of compressed air energy storage in salt formations.

I could not have done this project without the countless friends and labmates I have made during this project and may we hold each other up in the future as we have during this trial. In

particular, I would like to thank Matthew, Noga, Alix, Nicole, Mandy, Benjamin Gruber, Hélène, Soumi, and Anna for all of their hours talking about halite with me, and for their support when I needed it the most.

I am forever blessed by the mentors around me including Dr. Reed Scherer, Richard Lassin, Terry Briggs, and the E.S.C.O.N.I. organization for instilling a love of geology in me at a young age, for their support during my schooling, and most importantly for teaching me to ask better questions. Lastly, I would like to thank my parents who have always loved their geologist, even my collection of rocks filled precious space in the garage. Mom and Dad, thank you for all your support and unwavering belief in my potential.

# Table of Contents

## List of Tables



## List of Figures

## List of Plates

## List of abbreviations and symbols

| | |
|---|---|
| AB | Alberta |
| ASCII | American Standard Code for Information Interchange |
| CAB | Central Alberta Basin |
| cm | Centimeter |
| (d) | Modifier indicating diagenesis |
| e.g. | For example |
| EPB | Elk Point Basin |
| (f) | Flooding surface |
| Fm. | Formation |
| i.e. | That is, in other words |
| $g/cm^3$ | Grams per cubic centimeter (density) |
| gAPI | Gamma ray unit (API) |
| GE | Golden Embayment |

| | |
|---|---|
| GR | Gamma ray |
| $kg/m^3$ | Kilograms per cubic meter (density) |
| kV | Kilovolt |
| km | Kilometer |
| S-ICP-MS | Solution inductively-coupled plasma mass spectrometry |
| LA-ICP-MS | Laser ablation inductively-coupled plasma mass spectrometry |
| LAS | Proprietary file format |
| m | Meter |
| Ma | Million Years Ago |
| MN | Manitoba |
| mV | Millivolt |
| NAB | Northern Alberta Basin |
| Ohm | Unit for electrical resistance |
| ppm | Parts per million |
| RES | Resistivity |
| RHOB | Bulk density (corrected), $g/cm^3$ |
| (s) | Subaerial surface |
| SK | Saskatchewan |
| sl. | Silt sized particles |
| TVD | Total vertical depth |
| Vol. % | Volume percent |
| WM | Watt Mountain |
| WW% | Water weight percent |

| | |
|---|---|
| XRD | X-ray diffraction |
| Δinflux | Change in rate of water input |
| μm | Micrometer |
| μs/ft | Microsecond per foot |

# 1 Introduction

With improved scientific understanding and development of modern analytical techniques, study of evaporite deposits has evolved from modeling chemical successions (Borchert, 1969; Braitsch, 1971) and studying outcrops of insoluble material, to sedimentologic core studies paired with geochemical analysis (Schreiber et al., 2007; John K Warren, 2016).

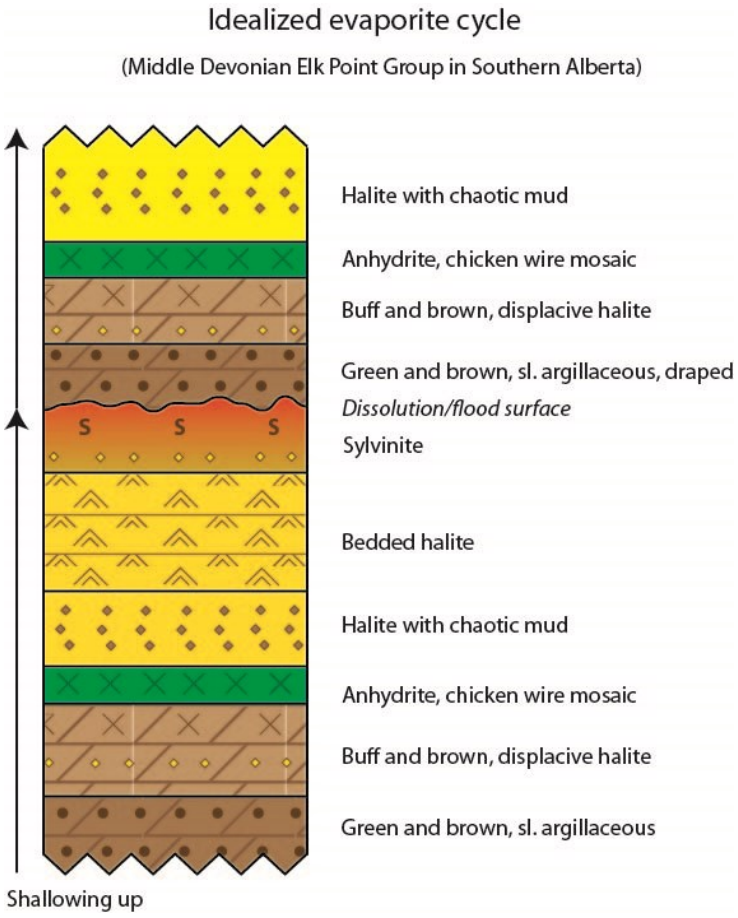


**Figure 1** Idealized evaporite depositional cycle for the Middle Devonian Central Alberta Basin. Sl. – silt sized grains

Influential evaporite studies such as Braitsch (1971), Kendall (1978), Lowenstein and Hardie (1985), Lugli (2009), and Warren (2016) identified the "normal" evaporite depositional sequence that transitions progressively vertically upward through carbonates, sulphates, halite, and potash.

(**Figure 1**). Understanding fluid chemistry and its effect on evaporite mineral precipitation (carbonate, gypsum, and halite) during evaporative concentration has been integral to expanding evaporite sedimentologic research in salt giants (Jones, 1966; Hardie and Eugster, 1970; Smoot and Lowenstein, 1991).

Salt giants are ancient evaporite deposits that can extend over thousands of square kilometers of map area in the subsurface, and record millions of years of geologic history. These units preserve soluble deposits that formed in the presence of inland epeiric seas, which are not expressed in outcrop or modern depositional environments (Hsü, 1972). Sedimentologic studies of salt giants rely upon vertical core description and correlation of drill cores, which are sometimes hundreds of kilometers apart. Widely separated drill cores hinder regional interpretation, as correlation and interpretation of lateral evaporite facies configuration becomes increasingly less certain.

The purpose of this study is to develop an approach for defining spatial relationships between salt facies with well log data and to apply this approach to the Elk Point Basin. Well log analysis for facies recognition and mapping is important because many ancient evaporite deposits are rarely cored but well log data is common. Several features must be considered to describe and analyze evaporite facies in a basin, including lithology, sedimentary fabrics, diagenesis, and the chemical composition of insoluble impurities in rock salt (Kendall, 2010; Lowenstein and Hardie, 1985; Lugli, 2009; John K. Warren, 2016). I propose a new method to identify and correlate facies between distant cores, by interpreting wire line logs. This method can be employed even in the case of poor core preservation or sparse core coverage. This method is based on new basin-wide correlation and drill core study that allows for an accurate prediction of marker beds and better paleo-environment interpretation and modelling across large distances.

In this study I describe sedimentologic findings and produce facies models of the Devonian Prairie Evaporite of south-central Alberta (Figure 2). The Prairie Evaporite Formation is a major evaporitic deposit in the Elk Point Group comprising deposits of Givetian strata (Holter, 1969; Sherwin, 1962). I interpret the facies distribution and depositional environments of the Elk Point Basin using new data of the Prairie Evaporite Formation but also building upon work completed by Brodylo (1987) on north Alberta Prairie Evaporite Formation deposits, Sherwin and Api (1962) on central Alberta Elk Point Group deposits, and Bebout (1973) on time-equivalent western Alberta anhydrite deposits (Muskeg Formation). The Prairie Evaporite formation was chosen for study due to the abundance of available published research, well log data, and drill core available, as well as the presence of primary salt and economic deposits such as potash, a group of K- and Mg-rich salts.

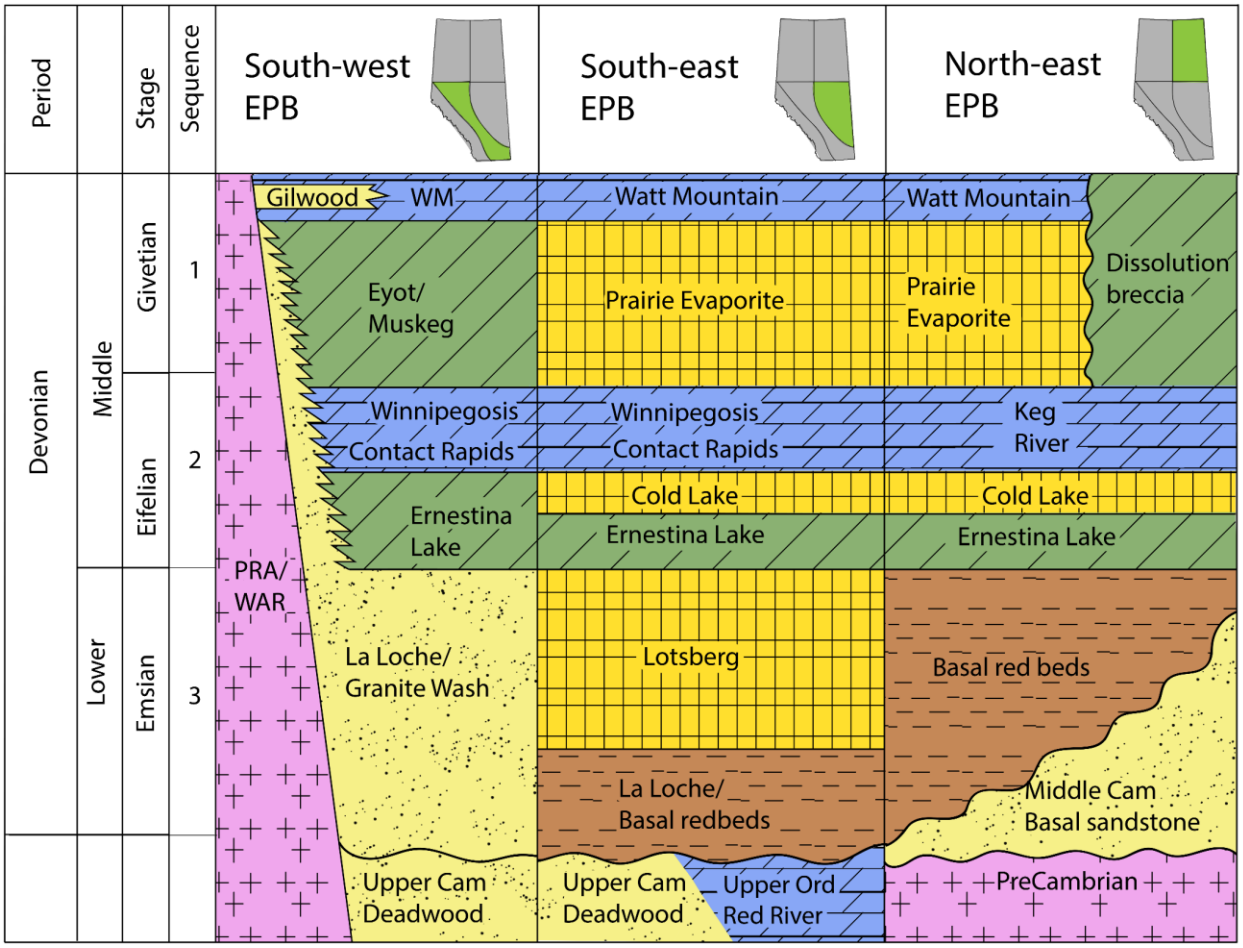


Figure 2: Stratigraphic section of the Elk Point Basin (EPB) for various portions of Alberta (indicated by highlighted green zones). After Hauck et al. (2017) and Drees (1994). Abbreviations: Cam = Cambrian, Ord = Ordovician. PRA = Peace River Arch, WAR = West Alberta Ridge, WM = Watt Mountain.

## 2 Geologic background

The Elk Point Group was deposited during the Early Devonian era on the western passive margin of Laurasia (Figure 3). Western Laurasia evolved into a convergent margin setting by the Middle Devonian (Domeier and Torsvik, 2014; Pysklywec and Mitrovica, 2000). During the Middle

Devonian, modern day Alberta was located on the western Panthalassic paleo-coastline. During the Devonian, the coastline trended NW-SE across the modern Alberta – British Columbia border (Cocks and Torsvik, 2011; Witzke and Heckel, 1988).

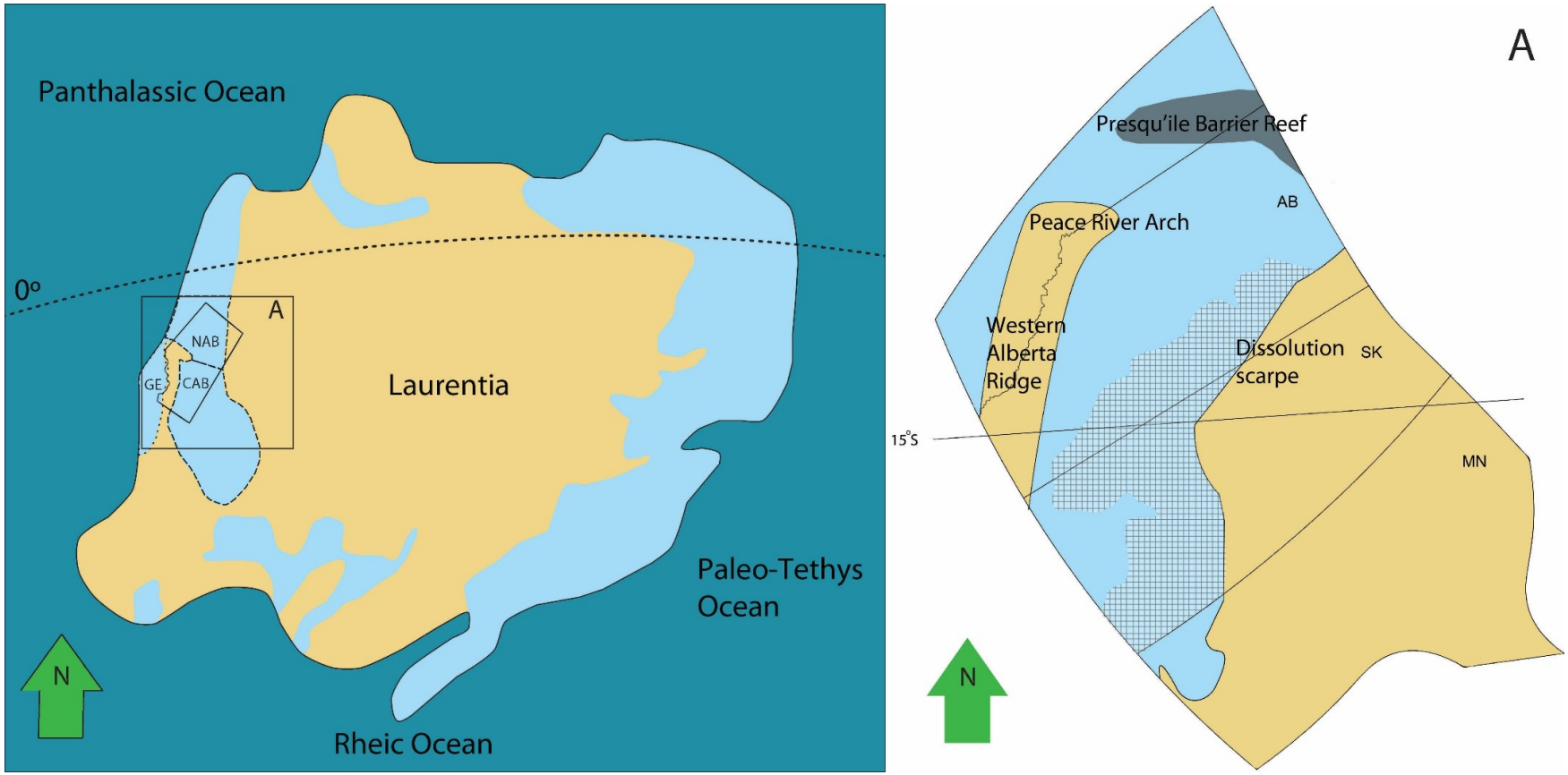


**Figure 3** LEFT: Paleo-reconstruction of the area of study during the Middle Devonian in the content of the Laurentian continent. Abbreviations: NAB = Northern Alberta Basin, CAB = Central Alberta Basin, GE = Golden Embayment (Scotese, 2001; Witzke and Heckel, 1988). RIGHT: Box A is a close-up of the left map, focusing solely on the Canadian provinces and emergent topographic features. The Presqu'ile Barrier Reef is highlighted with dark grey. Halite with > 90% purity is highlighted with cross-hatching (Grobe, 2000; Meijer Drees, 1994).

Emergent features such as the Presqu'ile barrier reef suggest small scale tectonism to the north west of the Central Alberta Basin that is not fully captured by the description of a passive margin. Global atmospheric temperatures and Panthalassic relative sea level reached a maximum during the Frasnian age in western Laurasia (Burrowes and Krause, 1987; Cocks and Torsvik, 2011). A series of basins formed along the continental margin due to pre-Devonian flexure and erosion, including the Elk Point Basin (Pysklywec and Mitrovica, 2000), which developed initially as Northern and Central Alberta sub-basins separated by the emergent Peace River Arch (Cant, 1988; Meijer Drees, 1994). The Central Alberta Basin was separated from the Golden Embayment by the Western Alberta Ridge (Meijer Drees, 1994). Post-burial tectonism in the basin tilted Central Alberta Basin deposits toward the southwest with a dip of~ 18º.

In this study I focus on the Central Alberta Basin, which extends across modern central and southern Alberta (Figure 3). During the Early Devonian, the Central Alberta Basin was isolated from the open ocean by the Peace River Arch and the Western Alberta Ridge to the south west (Meijer Drees, 1994). These topographic highs were local sources of siliciclastic sediment that are found interbedded within Elk Point Group salt deposits (Burrowes and Krause, 1987). The ancestral Peace River Arch is thought to be a tectonic uplift along reactivated Precambrian faults at the craton edge during the Silurian period (Burrowes and Krause, 1987). Along the axis of the Western Alberta Ridge lies the ancestral Cambridge arch (Andrichuk, 1951). Erosion during the Late Silurian and Early Devonian incised into Cambrian, Silurian, and Ordovician stratigraphy, producing the pre-Devonian Unconformity (Meijer Drees et al., 2002). Hydrologic communication between the Panthalassic Ocean and the Central Alberta Basin was intermittent during the Devonian due to repeated marine eustatic fluctuations (Williams, 1984). During the early

Devonian, seawater was restricted from the Central Alberta Basin by the Peace River Arch to the north and the Western Alberta Ridge to the south-west (Figure 3).

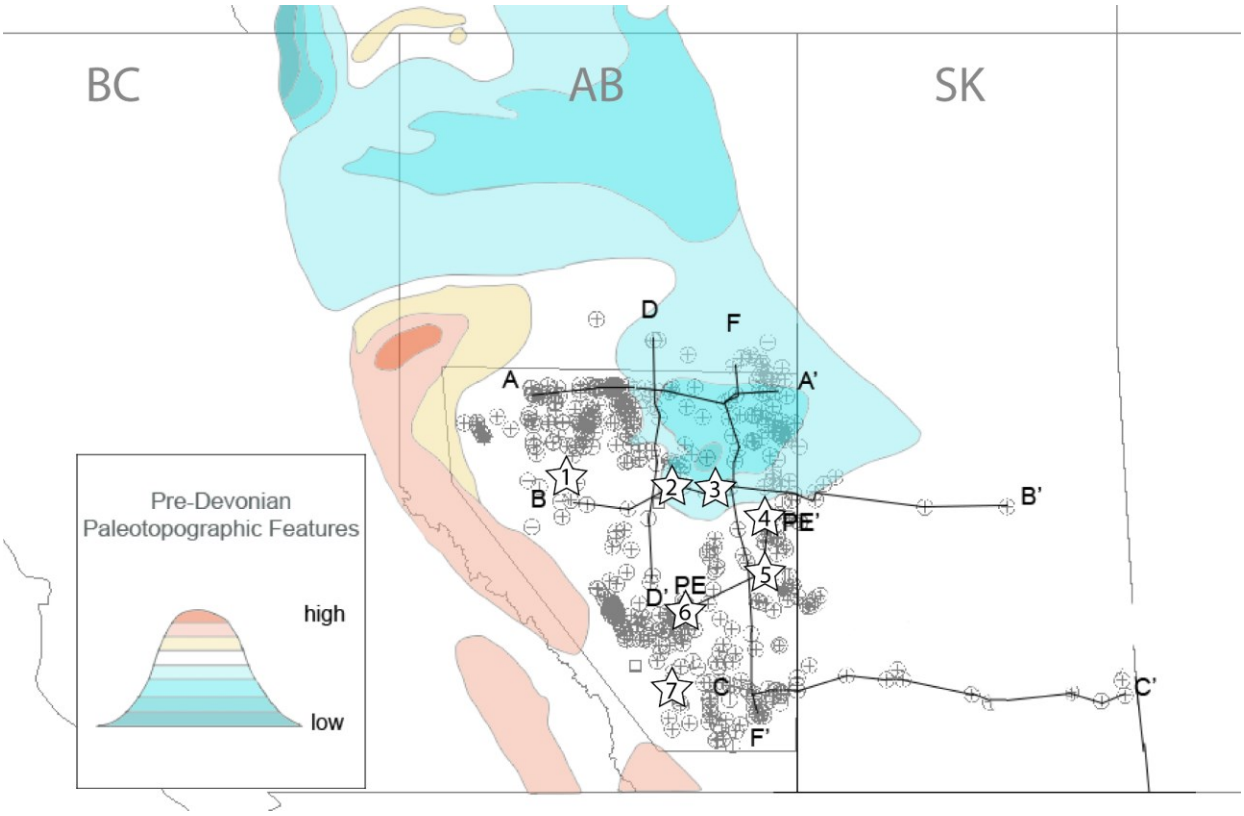


**Figure 4** Pre-Devonian paleotopography across the study area. Paleotopography after Drees (1994) combined with new data from this study. Cross sections AA', BB', CC', DD', FF', and PEPE' are indicated. Stars containing the numbers 1 through 7 indicate studied core locations. Wells in the study area are indicated by crosses inside of circles. Wells in Saskatchewan are used to develop regional E-W cross-sections.

Burial of the Peace River Arch combined with a contemporaneous relative sea level rise permitted flooding of the Central Alberta Basin from the start of the Middle Devonian onwards (Rogers, 2017). Subsequent growth of the Presqu'ile barrier to the north (Figure 3**Figure 4**) again restricted water communication between the Central Alberta Basin and the ocean, forming an epeiric sea (Klingspor, 1969; Maiklem, 1971). The Lotsberg, Ernestina Lake, Cold Lake, Contact Rapids, and Winnepegosis Formations were deposited by this epeiric sea. These units filled the lowest depression in the Central Alberta Basin and buried the Peace River Arch by the Middle Devonian (Meijer Drees, 1994).

Elk Point Group deposits in the Central Alberta Basin (Figure 2) overlie the Pre-Devonian Unconformity and therefore sit unconformably atop either crystalline Precambrian bedrock or Cambrian-Silurian sediments based on the nature of erosion in an area (Gussow, 1957; McCabe, 1954). During periods of arid climate and marine water source, the balance between water input flux and evaporation produce a predictable vertical depositional sequence of limestone, gypsum, halite, and potash (Wenk and Bulakh, 2016). Three evaporative sequences consisting of these lithologies are present in the Elk Point Group (Figure 2) containing up to 700 m of salt in combined thickness near the depositional center of the Central Alberta Basin (Grobe, 2000). Sequence 1 is comprised of, in ascending order, the basal red beds composed mainly of mudstone and the overlying the Lotsberg Formation composed mainly of halite. Sequence 2 is comprised of the Ernestina Lake Formation composed of mainly marlstone and the overlying Cold Lake Formation composed of halite and mudstone. Sequence 3 is comprised of the Winnepegosis Formation composed of dolostone and limestone, the Contact Rapids Formation composed of clastics and limestone, the Keg River Formation composed of dolostone and limestone, and the Prairie Evaporite Formation composed mainly of halite.

From the Middle Devonian to present, the Central Alberta Basin, and by extension the Prairie Evaporite Formation, has experienced isostatic flexure, dissolution collapse to the northeast and southwest, widespread dolomitization, and orogenic flexure. Chronology of the Central Alberta Basin is complex due to a multistage history involving evaporite deposition, diagenesis, and burial in the Elk Point Basin are convoluted and many times multistage processes. From the Early Devonian to the Cretaceous, the northwestern continental margin of Laurasia remained largely tectonically inactive. It is thought that during this quiescent period, fluid interaction in the basin lead to dissolution of salts and dolomitization of limestone along lineaments related to

flexure of the Western Canadian Sedimentary Basin trough (Broughton, 2013). Dissolution and alteration of halite occurred at least once before the Cretaceous, during a major event recorded during the Late Paleozoic around 300 Ma (Koehler et al., 1997). Late Jurassic-Early Cretaceous plate convergence produced tectonic thickening during the Cordilleran orogeny along the continental margin, and accompanying isostatic flexure which created a foreland basin that extended from North Dakota to the North Western Territories. A second major dissolution event took place during the Cretaceous (~ 60 Ma), and collapse of overlying strata replaced the Prairie Evaporite Formation with the development of breccia to the northeastern North Alberta Basin along the dissolution scarp and in the southeastern Central Alberta Basin. The Central Alberta Basin was then filled with Middle Jurassic and Cretaceous clastics during the erosion of the Cordillera (Leckie, 1986; Cant, 1988; Pana et al., 2001).

# 3 Dataset and methods

## *3.1 Core logging and well logs*

This study combines data from seven drill cores and logs for 975 wells that penetrate the Elk Point Group (Figure 2, Figure **3**, and Figure **4**; Appendix A). These data are used to produce and compare regional isopach maps and stratigraphic cross sections for the central Alberta basin. All logs were retrieved from the geoSCOUT database and access to cores was obtained from the Alberta Energy Regulator Core Research Center, Calgary, Canada.

For all cross-sections, the top of the Watt Mountain Formation has been chosen as the datum due to the flat nature of this clastic and carbonate deposit and the reliability of its correlation across the Central Alberta. I refer to cores by abbreviated identifiers in this study (Table 1).

**Table 1** Details for cores and core logs in this study. All wells listed below are vertical

| Core ID | Formation | Length of core (m) | Latitude (N) | Longitude (W) | In-text identifier |
|---|---|---|---|---|---|
| 100/16-33-040-07W4/00 | Prairie Evaporite | 110 | 52º29’20.7960” | 110º56’45.9960” | #1 |
| 100/14-14-055-15W4/00 | Prairie Evaporite | 14 | 53º45’25.1280” | 112º07’27.6601” | #2 |
| 100/06-12-049-06W4/00 | Prairie Evaporite | 133 | 53º12’41.2200” | 110º45’12.0239” | #3 |
| 100/15-30-034-20W4/00 | Prairie Evaporite | 45 | 51º57’14.0760” | 112º49’34.7160” | #4 |
| 100/13-09-064-26W5/00 | Gilwood | 26 | 54º31’39.4320” | 117º52’43.5360” | #5 |
| 100/01-33-07-03W4/00 | Prairie Evaporite | 112 | 52º12’59.4000” | 110º21’49.2839” | #6 |
| 100/10-11-020-24W4/00 | Gilwood | 150 | 50º40’59.7720 | 113º13’19.3800” | #7 |

### *3.2 Core Description*

Cores were logged at centimeter-scale for lithology, interstitial clay content (vol. %), crystal size, and other key features including dissolution vugs, crystal form (i.e., chevron, anhedral, fibrous,

etc.), insoluble beds and lenses, displacive halite in mudflat beds, milky halite, and the presence of potash. Crystal size was measured across the largest diameter on a representative crystal and split into three size groups: 0-7 cm, 7-13 cm, >13 cm. The range of sizes was recorded where crystal sizes were heterogeneous.

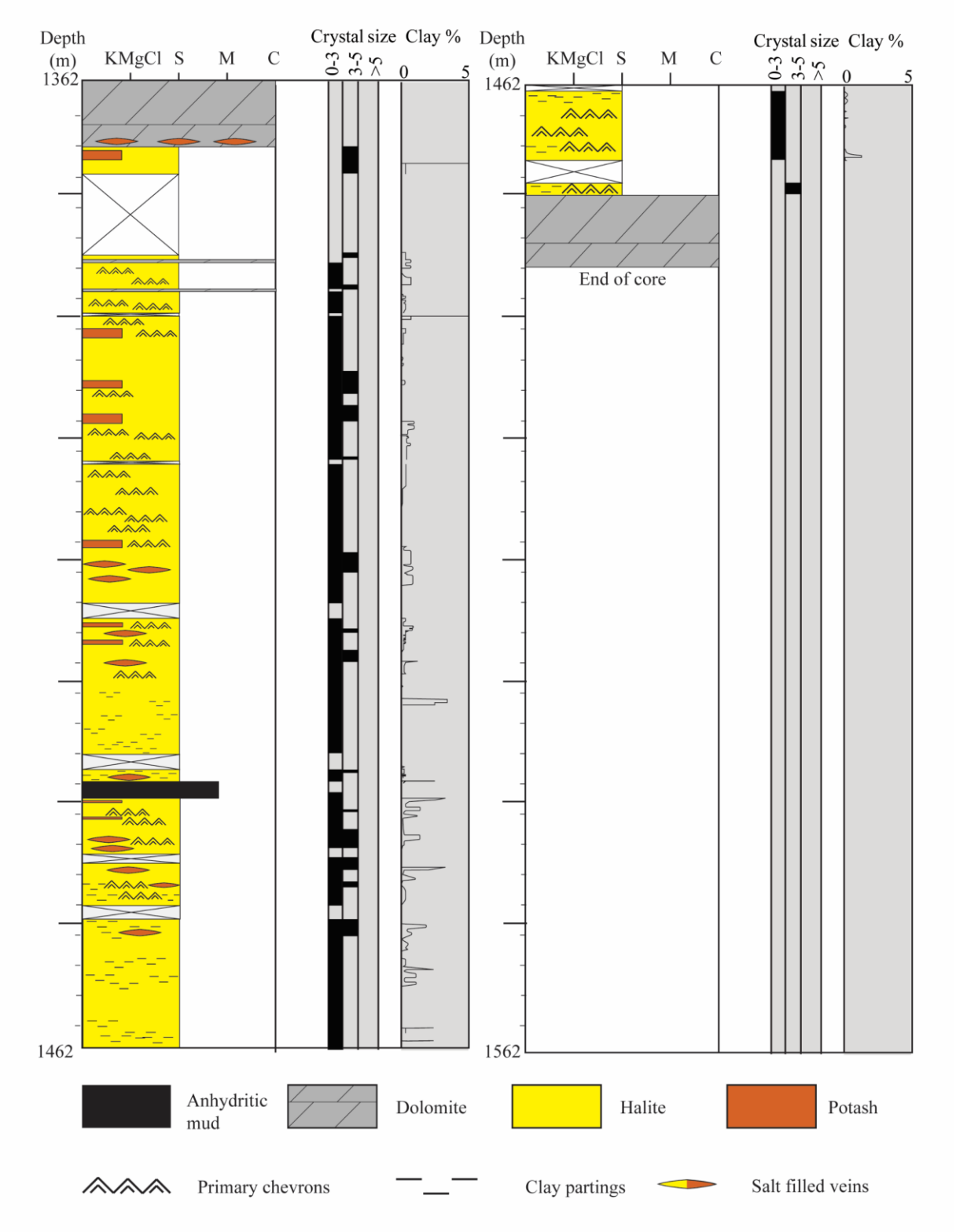


**Figure 5** Core log of Well #1 depicting lithology, sedimentary features, and clay %

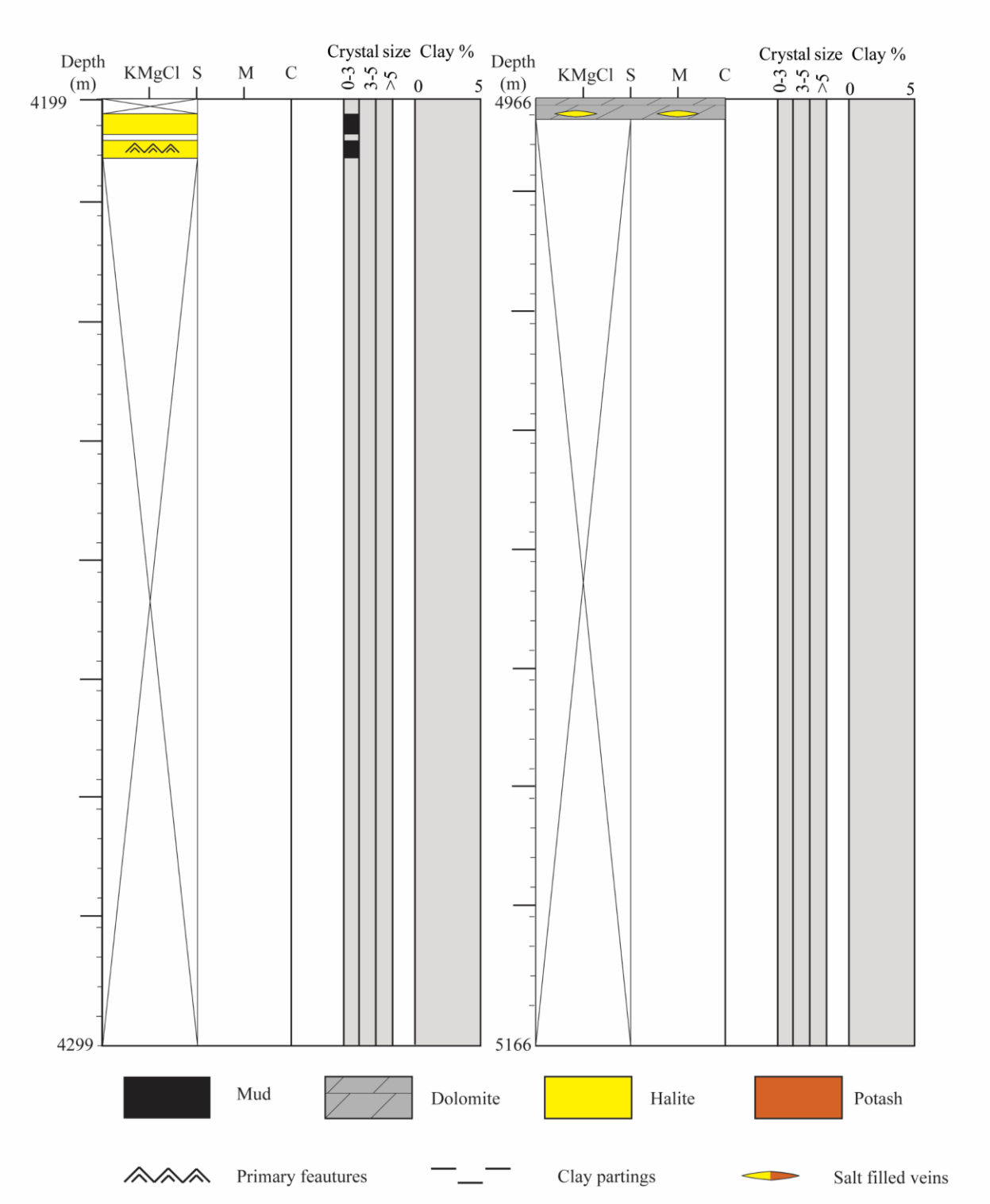


**Figure 6** Core log of Well #2 depicting lithology, sedimentary features, and clay %

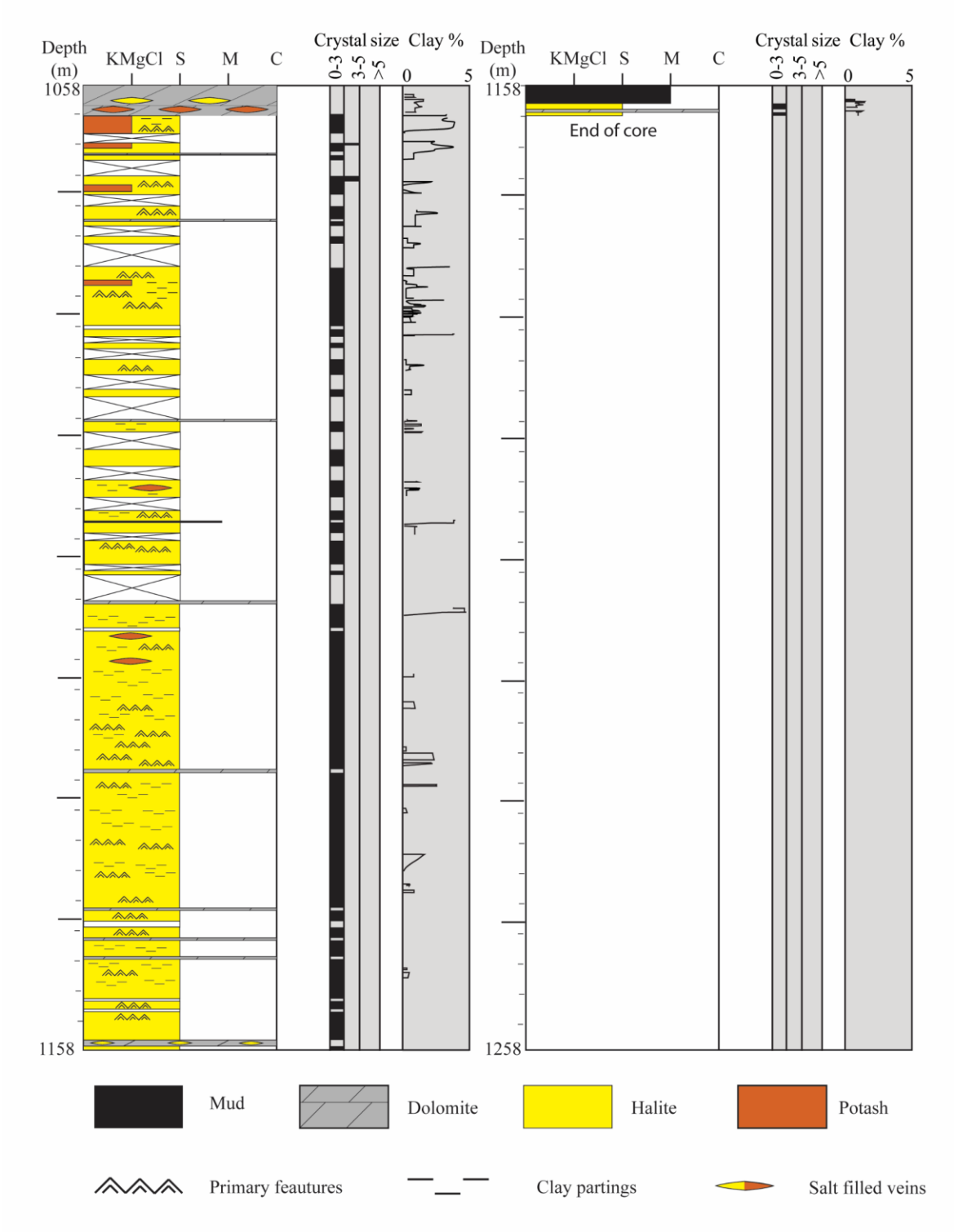


**Figure 7** Core log of Well #3 depicting lithology, sedimentary features, and clay %

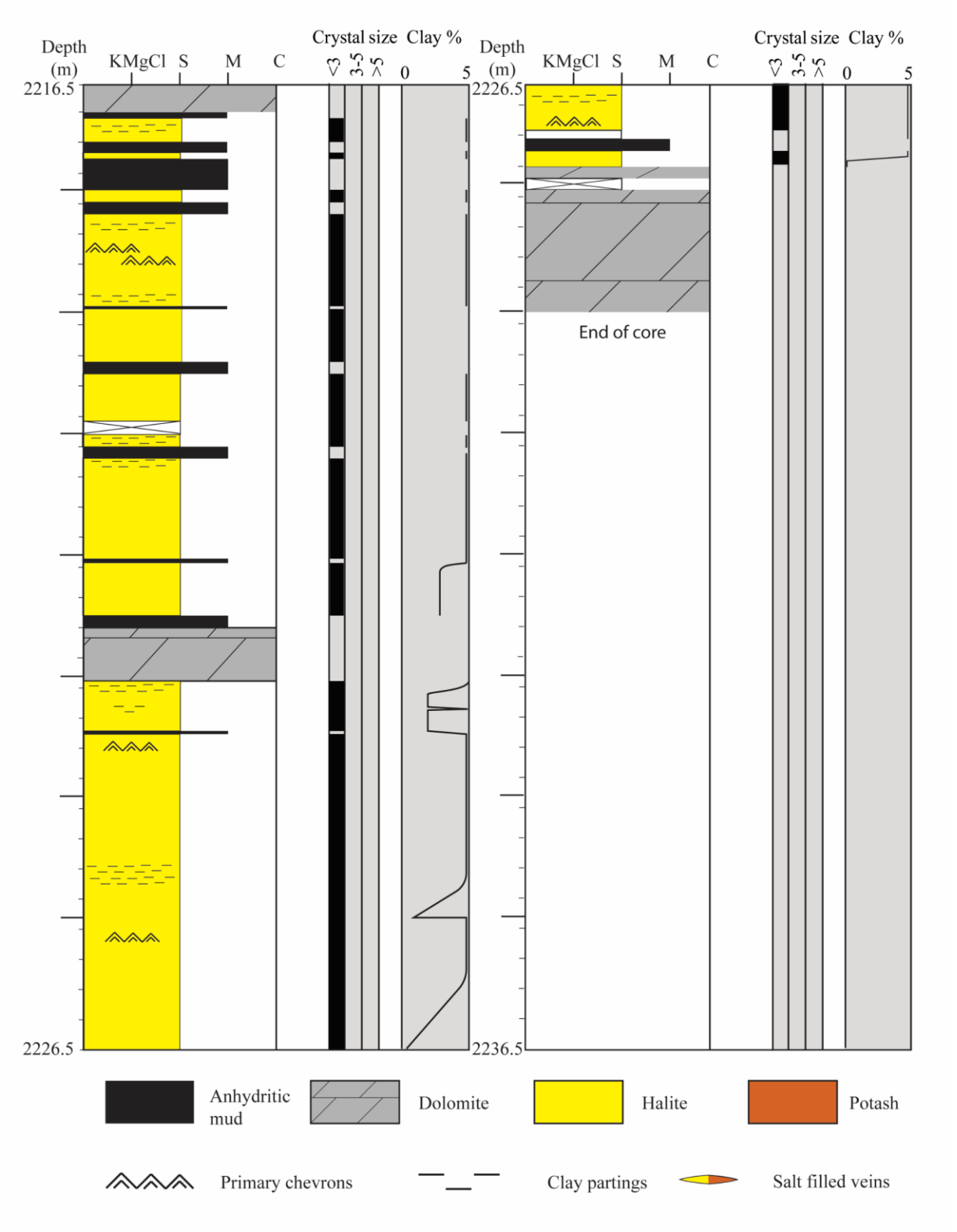


Figure 8 Core log of Well #4 depicting lithology, sedimentary features, and clay %

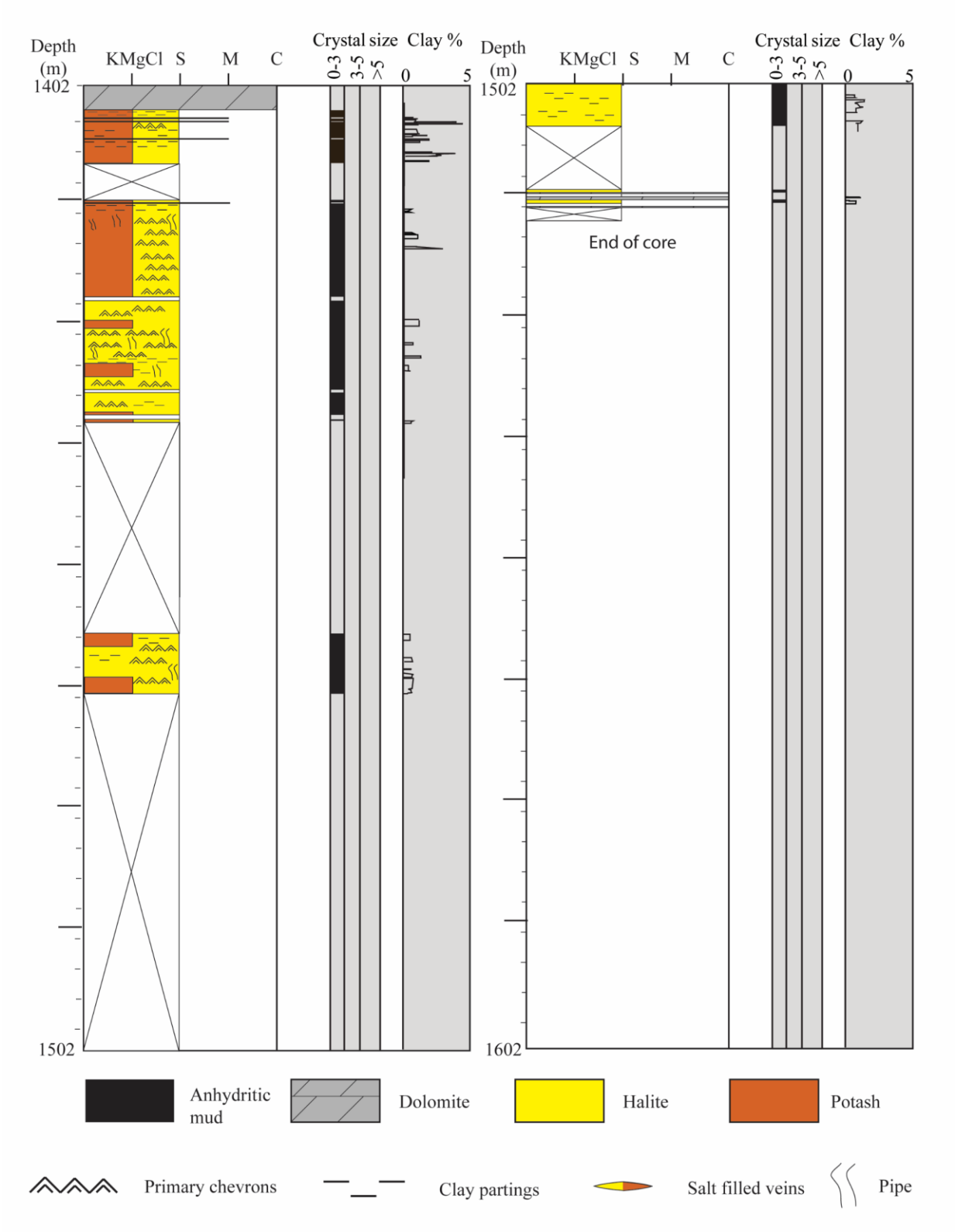


**Figure 9** Core log of Well #6 depicting lithology, sedimentary features, and clay %

### *3.3 Well Log Interpretation*

Basin-wide interpretation of lithology from well logs is only applicable to wells containing log ASCII standard (LAS) curves. Cutoffs listed in Table 2 are used to define bulk lithology.

**Table 2** Typical well log values used to identify lithologies in this study (Crain and Anderson, 1966)

| Lithology | GR (GAPI) | RHOB (g/cm$^3$) | RES (ohm) |
|---|---|---|---|
| Halite | n/a | 2.00 | >1000 |
| Anhydrite | n/a | 2.8 | High |
| Dolostone | n/a | 2.6 | Medium |
| Sylvite | 100 | 1.8 | > 500 |
| Sandstone | n/a | 2.0 | < 300 |

Logs were sourced from geoSCOUT for 602 wells within Alberta, and 373 wells in Saskatchewan totaling 975 well logs (Appendix A). LAS files are higher quality and report information at < 1 m resolution compared to image files of paper logs (raster logs) which commonly have a minimum resolved thickness of two meters. Both LAS and raster files are imported into Petrel and associated with the correct well, after which depth-shifting and interpretation are completed.

### *3.4 Core to Log Correlation*

Core descriptions are compared to well logs and depth-shifted to total vertical depth (TVD). Core depth is best corrected by matching observed core lithology to the density log. Where density logs are unavailable, I use the caliper and deep resistivity logs.

### *3.5 Core sampling and sample preparation*

Four cores were chosen for sample analysis based on penetration of the Prairie Evaporite Formation as well as core length covering the thickness of the formation (Table 3). I selected samples based on a variety of criteria, including distinctive colors and lithologies or unique fabric. Slabs were cut 6.5 cm long sampled at least two feet apart, using a 25.4 cm diameter circular

diamond-coated rock saw using propylene glycol lubricant. A 1 cm-wide strip was cut from the side of each slab and powdered using a Retsch RM 200 grinder for 3 minutes.

### *3.6 XRD analysis*

X-ray diffraction (XRD) analysis of core samples was completed at the University of Alberta using a Rigaku Ultima IV diffractometer with a Cobalt tube at 38 kV and 38 mA. The detector was a D/Tex Ultra with Fe filter using Bragg Brentano Mode focusing geometry. Slit sizes used were 2/3° divergence slit, 10 mm divergence height limiting slit, open scattering slit, and open receiving slit. The range of the scan was 5 to 90º with a continuous scan mode using a 2θ/θ axis at 2 °/min and 0.0200º step size. Each sample powder was prepared using the Top-Pack method on a Rigaku Top-Pack 24mm sample holder. Data interpretation was done using Jade 9.6 software with the 2019 ICDD Database PDF 4+, and 2018-1 ICSD databases.

## 4 Results

### *4.1 Facies*

Preserved sedimentary features within evaporite deposits record the paleo-depositional, paleo-environmental and early diagenetic histories of a basin. The following features are observed within the Elk Point Group salt bodies: bedding, foundered cumulates, chevron crystals, mud drapes, dissolution beds, and haloturbation (Plates 1 through 9). Common stratigraphic surfaces within facies are flooding surfaces and subaerial exposure. Evidence for diagenesis overwrites primary fabrics, remobilizes soluble minerals, and alters mineral structures into more stable forms (e.g., gypsum to anhydrite). These characteristics are amended as modifiers to facies where observed.

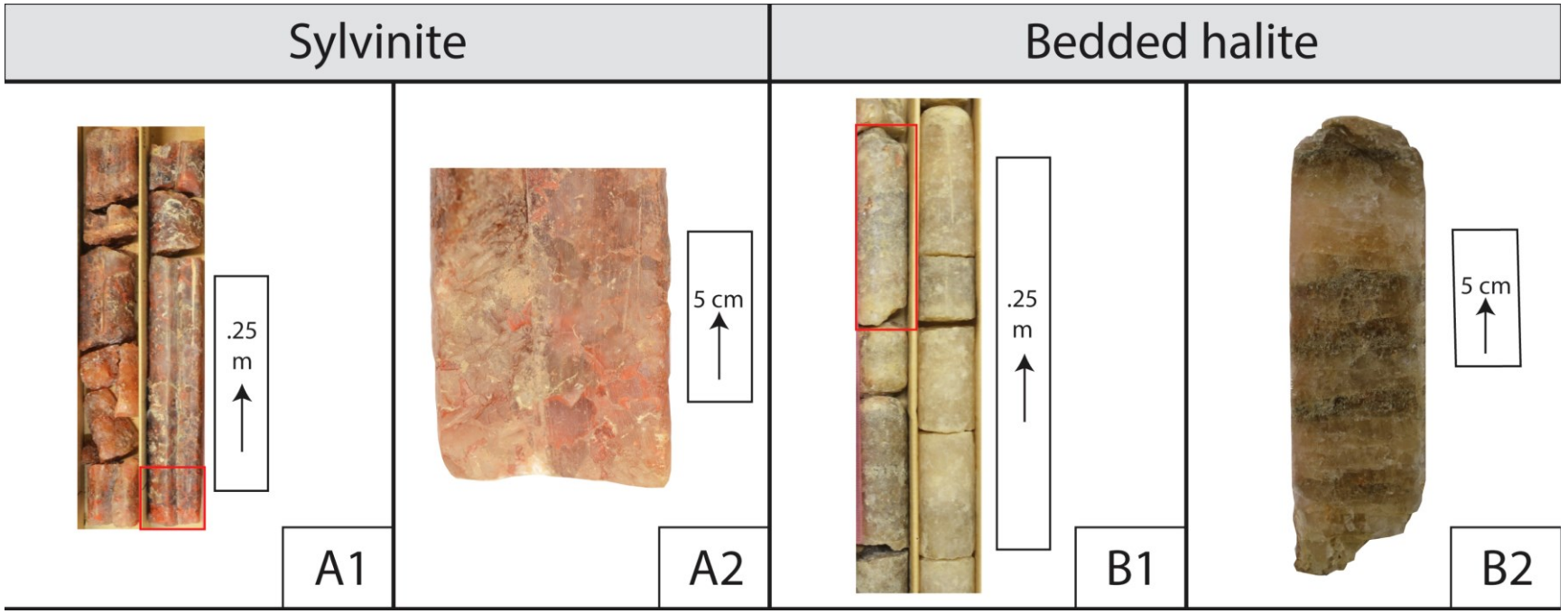


**Figure 10 A and B** Photographs of core for the Prairie Evaporite Formation, subdivided based on interpreted facies. Red box shows extent of enlarged photo. See text for (section 4.1.x) full description.

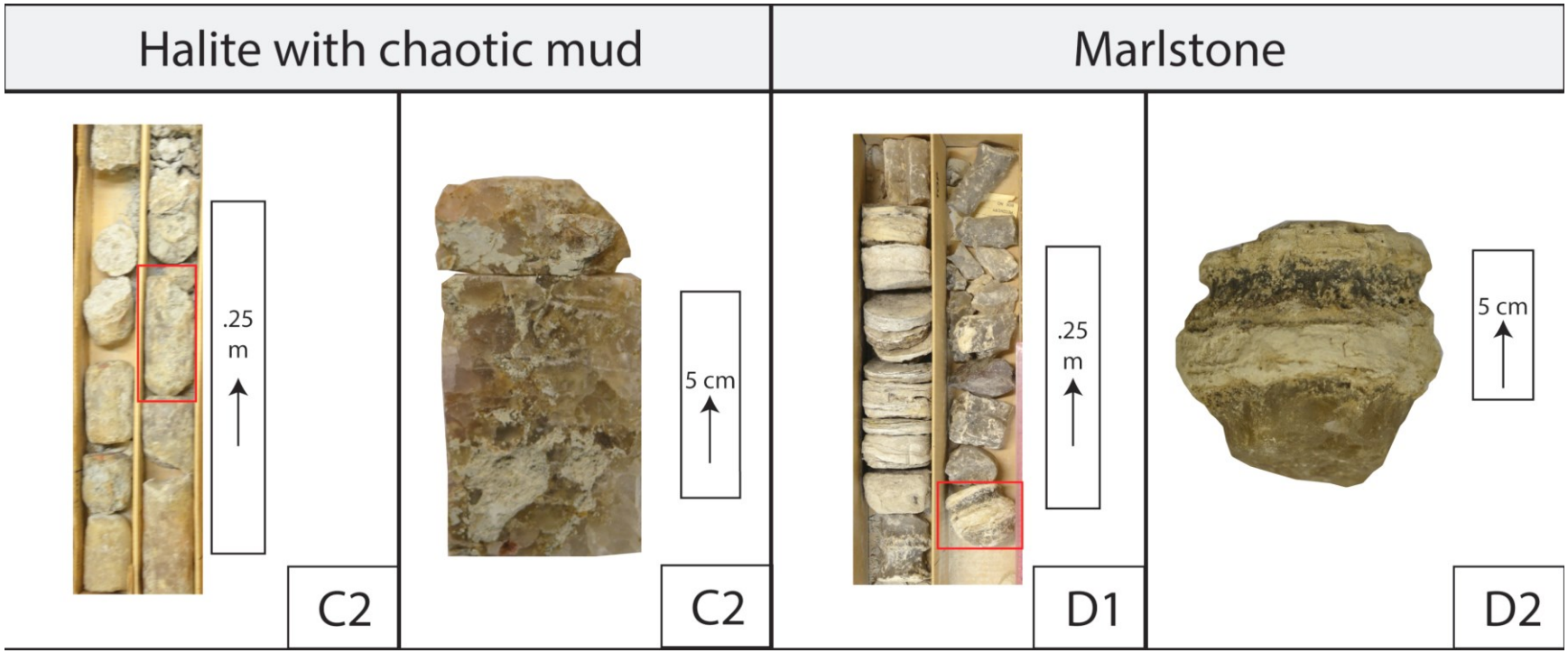


**Figure 10 C and D** Photographs of core for the Prairie Evaporite Formation, subdivided based on interpreted facies. Red box shows extent of enlarged photo. See text for (section 4.1.x) full description.

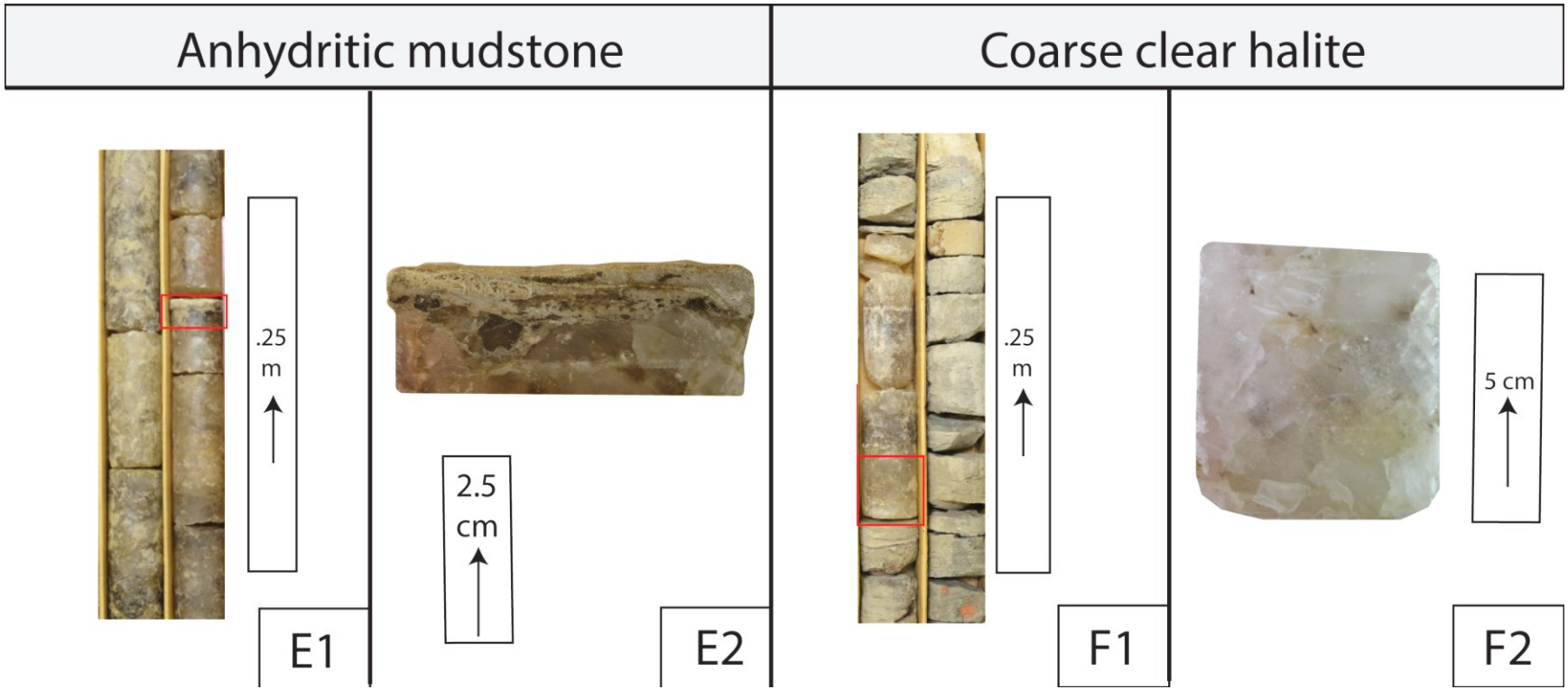


**Figure 10 E and F** Photographs of core for the Prairie Evaporite Formation, subdivided based on interpreted facies. Red box shows extent of enlarged photo. See text for (section 4.1.x) full description.

### 4.1.1 Sylvinite

The sylvinite facies is composed dominantly of < 7 cm and 7-13 cm diameter grey to maroon halite crystals, depending on the composition and quantity of dispersed mud (Figure 10A; Table B1). Sylvite cement was deposited in vugs and interstitial pore space between halite crystals. This secondary sylvite occurs as either massive metallic red or zoned (bright red rim to milky center) crystals (Broughton, 2019). Sylvite crystals adjoin surrounding halite with a wavy crystal boundary. Sylvinite beds (5 cm to 1 m thick) cycle between potash-rich (~ 3-5% sylvite) and -poor (< 3% sylvite), but no primary fabrics are present within these potash deposits.

### 4.1.2 Bedded halite

Bedded halite deposits are composed of clear, grey, and pink halite crystals < 13 cm in diameter with minor (< 3 %) interstitial clay (Figure 10B; Table B1). Bedding commonly occurs as zones of clear to grey halite separated by dissolution surfaces, which are marked by truncated chevron crystals, pipes, vugs, and occasional anhydrite drapes with variable clay content. Remnant bottom growth chevron fabrics are apparent, though the fabric surface is often discontinuous within the diameter of the core. Dissolution condenses the insoluble portion (i.e., clay, anhydrite, dolomite) of dissolved halite beds into pipes and vugs as either a lining surrounding bedded halite or intermixed with halite as chaotic mud.

Both ‘lightly-altered’ and ‘heavily-altered’ variants are present in the bedded halite facies. Lightly-altered halite is defined by halite with 7-13 cm crystal diameter with wavy intergranular boundaries intersecting at approximately 120º. Features such as major beds and fabrics, and color

imparted by intercrystalline impurities are partially retained. Heavily-altered halite contains little to no trace of primary beds or primary halite fabrics. When primary fabrics are pervasively recrystallized, bedding is preserved as a cycle of insoluble-free, white halite transitioning upward through maroon halite terminating upwards onto a condensed insoluble layer consisting of a mixture of insoluble content from the dissolved thickness of halite (f).

#### 4.1.3 Halite with chaotic mud

Halite with chaotic mud deposits are dominantly composed of < 7 cm grey to maroon halite crystals with ~ 3-5 % interstitial clay (Figure 10C; Table B1). Halite with chaotic mud occurs as grey, maroon, or dark brown zones with flat dissolution surfaces presenting as condensed bedding, associated with condensed beds of insoluble material. Diagenesis of halite with chaotic mud presents as compaction of anhydritic mudstone nodules around recrystallized halite crystals with recrystallization induced wavy boundaries. These nodules present as insoluble stringers in thin beds, whereas thick beds tend towards homogenous massive bedding.

#### 4.1.4 Coarse clear halite

The defining feature of this facies is > 13 cm clear – transparent pink halite crystals with triple junctions at 120º (Figure 10D; Table B1). Coarse clear halite is typically deposited within and adjacent to dissolution surfaces such as pipes and vugs. Dissolution pipes and vugs may be filled in with bedded coarse clear halite separated by truncation boundaries. Fluid inclusions tend to be large but low in abundance. Diagenetic features include oblate crystals or straight crystal boundaries with 90º junctions. Cyclic deposits are preserved as clear halite transitioning upward through transparent pink halite terminating upwards with a condensed insoluble layer.

### 4.1.5 Anhydrite-rich mudstone

Anhydritic mudstone deposits are dominantly composed of microcrystalline anhydrite with minor dolomite, calcite, and clay (Figure 10E; Table B1). This facies is composed of laminated to massive beds of light green grey – dark grey and light buff – medium brown mudstone depending on the relative abundance of anhydrite, dolomite, and clay. The mudstones occur as > 25 cm thick beds of variable clay content between saline evaporate deposits. Diagenetic features resent in studied core are mosaic nodules and wavy lamination.

### 4.1.6 Marlstone

The marlstone facies is composed of laminated to massive beds of light green grey, light buff – medium brown, and/or maroon microcrystalline marlstone (Figure 10F; Table B1). Common features include intraclast smearing (haloturbation), displacive-halite-filled mudstone, casts of cumulate beds, brecciation, and fractures filled with red fibrous halite. When occurring directly above bedded halite deposits, marlstone deposits preserve casts of halite chevron growth.

## *4.2 Log identification of the facies*

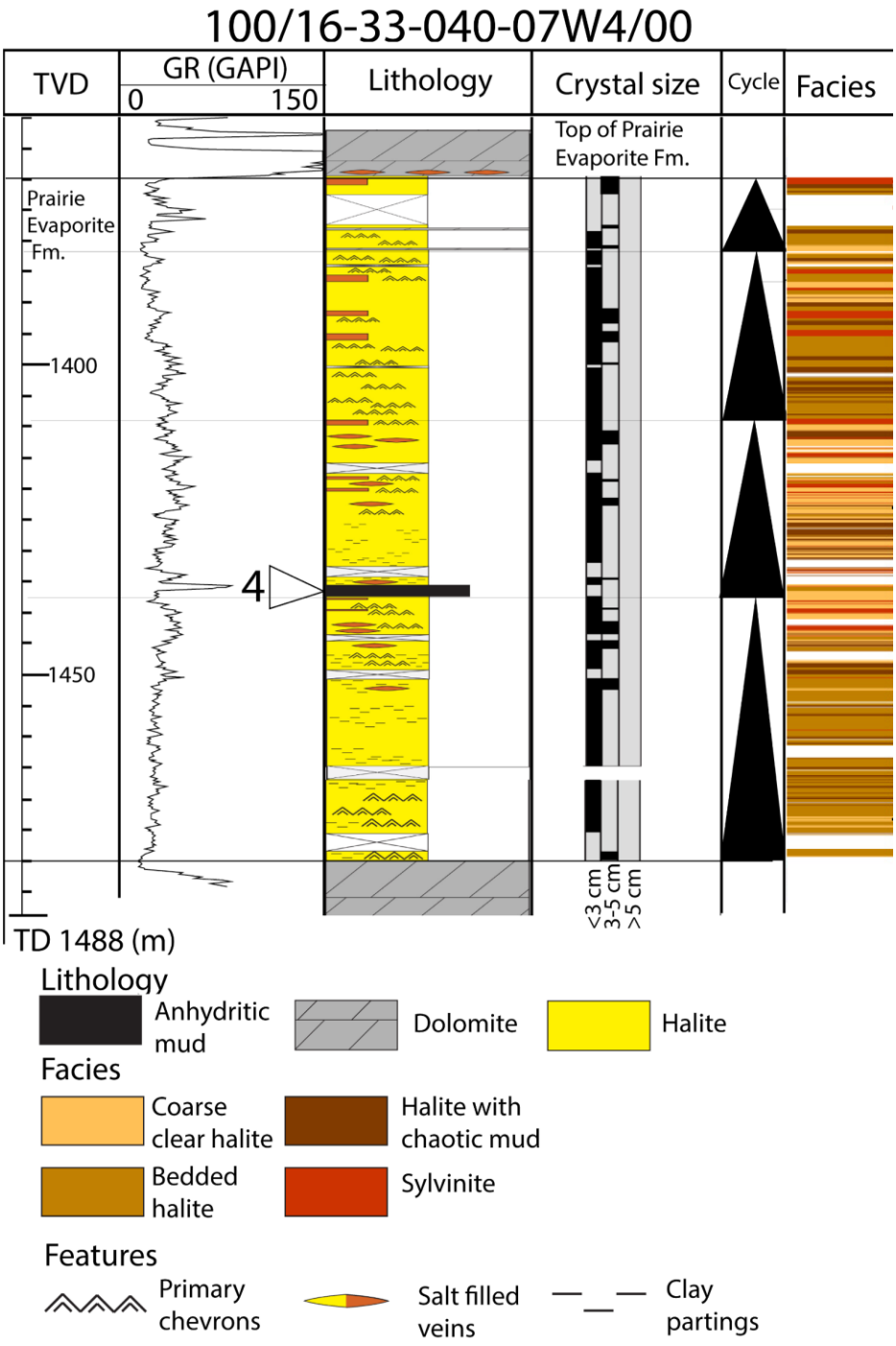


**Figure 11** Facies to core log connection in the Central Alberta Basin from Well #1 drill core. Triangles within the Cycle column indicate the evaporate sequences (Figure 1). The empty triangle labelled "4" indicates the depth of the marker bed of Cycle 4. Abbreviations: GR = gamma ray, TVD = total vertical depth.

Evaporite facies seen in core are correlated with well log features to produce a calibrated wireline facies identification scheme for the Central Alberta Basin (Figure 11). Halite is recognized by low density, near infinite resistivity, and in most cases borehole washout. The non-salt top and bottom of the Prairie Evaporite Formation as well as interbeds within, are recognized in logs by increased density, decreased resistivity, and sharp changes in caliper width due to dissolution resistance.

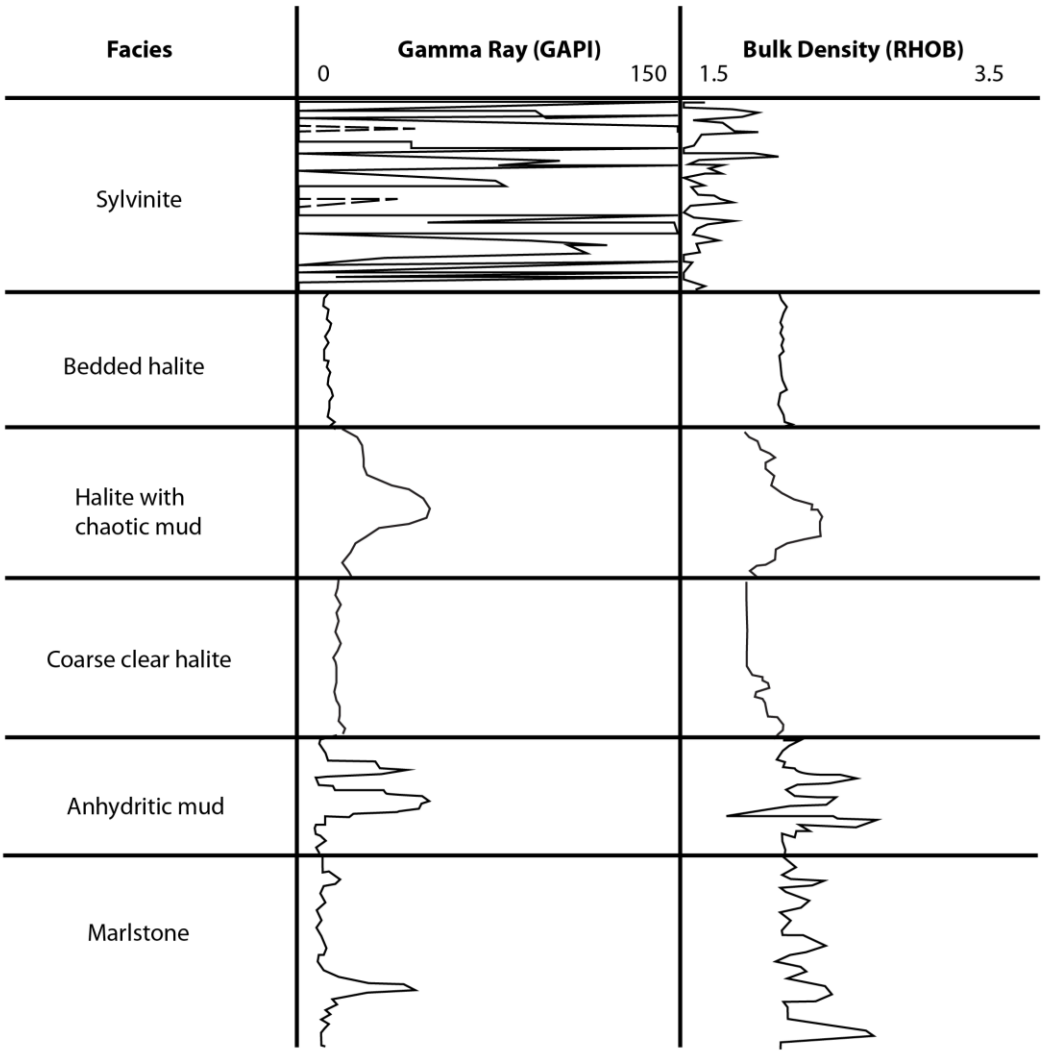


**Figure 12** Characteristic gamma ray and bulk density signals for facies in this study

Washout commonly occurs in boreholes due to the use of low-salinity drilling fluids, this requires borehole compensation in well logs which was not applied to the majority of raster well logs used in this project. Borehole washouts shift log responses from true values, as such the cutoffs used to interpret logs are apparent values (Figure 2, Figure 12, Table 3).

**Table 3** Characteristic well log features for facies in this study

| **Facies** | **GR (GAPI)** | **RHOB (g/cm$^3$)** | **RES (ohm)** |
|---|---|---|---|
| Sylvinite | 100-350 | 1.7-2.0 | High |
| Bedded Halite | 30-50 | 2.0-2.2 | $x \rightarrow \infty$ |
| Halite with Chaotic Mud | 30-80 | 2.1-2.3 | High |
| Bedded Halite with Dissolution Pipes and Vugs | 30-50 | 2.0-2.2 | $x \rightarrow \infty$ |
| Anhydritic Mudstone | 50-80 | 2.6-3.0 | Low-medium |
| Marlstone | 30-100 | 2.3-2.7 | Low-medium |

### *4.3 Spatial distribution*

Study of the spatial distribution of facies across the basin provided insight into large-scale cycles (tens of meters thick) within salt formations bounded by insoluble beds (Figure 11), described below in Section 4.4. The maximum halite thickness (190 m) of the Prairie Evaporite Formation is in the northeast of the study area and decreases to zero-thickness to the west and south along (Figure 13). The Prairie Evaporite Formation in the Central Alberta Basin transitions from ≤ 20 % halite in the west to > 90 % halite in the east (Figure 14, Figure **15**, Figure **16**, and Figure **17**).

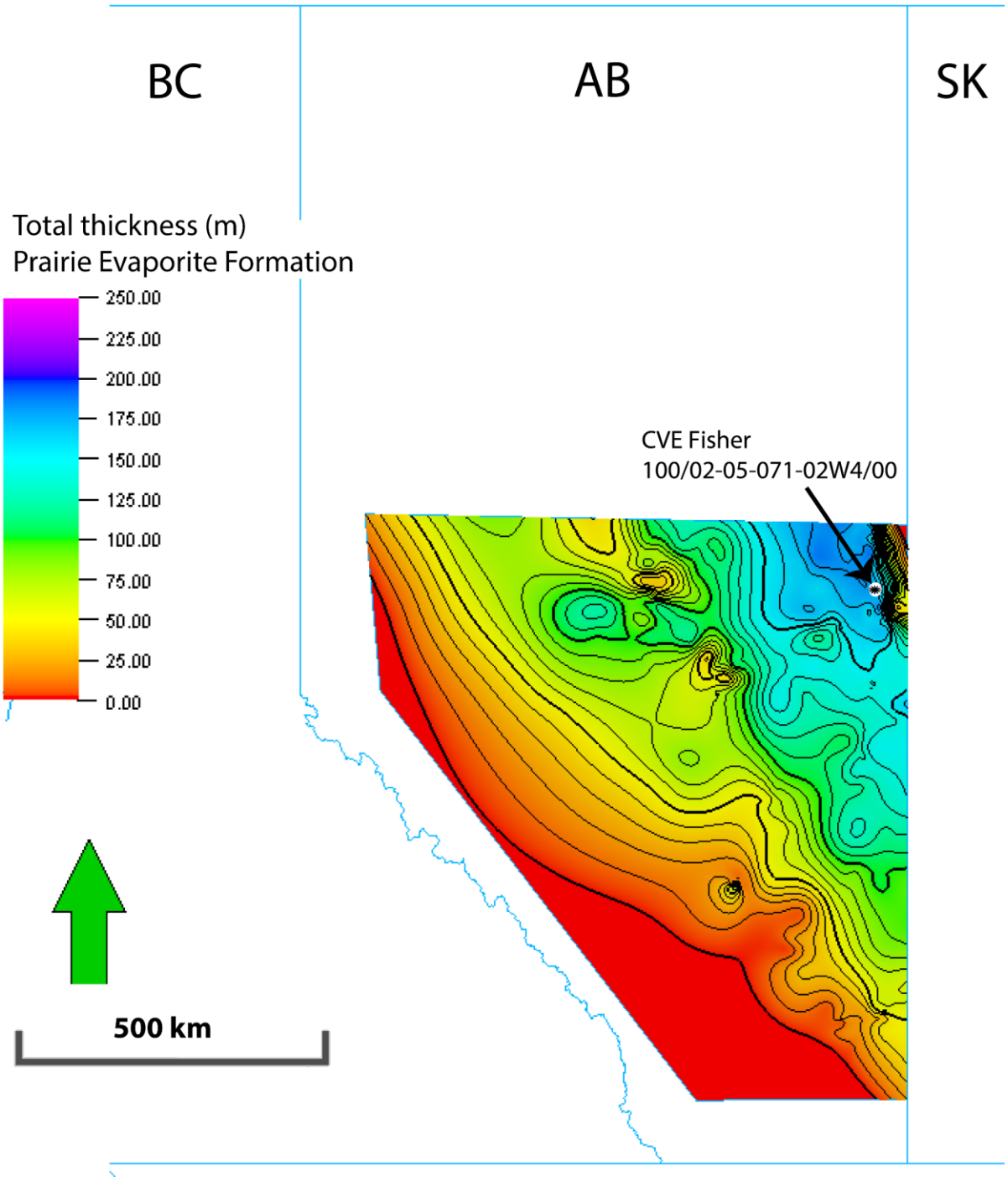


**Figure 13** Prairie Evaporite Formation net thickness map for the study area. Well CVE Fisher 100/02-05-071-02W4/00 shown.

A small-scale thinning feature is observed at the modern Alberta – Saskatchewan border, in which the Prairie Evaporite Formation rapidly decreases in thickness from 175 m to 70 m thick on the

net thickness map (Figure 13), represented in the well CVE Fisher (100/02-05-071-02W4/00), the location of which is shown in Figure 13. Where this thinning structure is observed, the top half of the Prairie Evaporite Formation is absent, due to either non-deposition or removal of halite, but the lowermost part of the formation is congruent with and proportional to nearby wells. The combined thickness of insoluble material within the Prairie Evaporite Formation is thickest to the northwest near the Peace River Arch (Figure 16).

### *4.4 Facies cycles*

Evaporation cycles are identified by an uppermost bounding insoluble marker bed. A facies cycle starts with anhydrite-dolomite-clay at the base, overlain by halite with chaotic mud, followed by bedded halite, to sylvinite (**Figure 1**) (Andrichuk, 1951; Bąbel and Schreiber, 2014). Any description of cycles herein refers to this sequence of deposits, whether partial or complete. Incomplete vertical cycles are considered sub-cycles, and tend to lack horizontal continuity between wells over distance. As such, seven cycles containing widespread marker beds are described below, starting with the lowermost cycle.

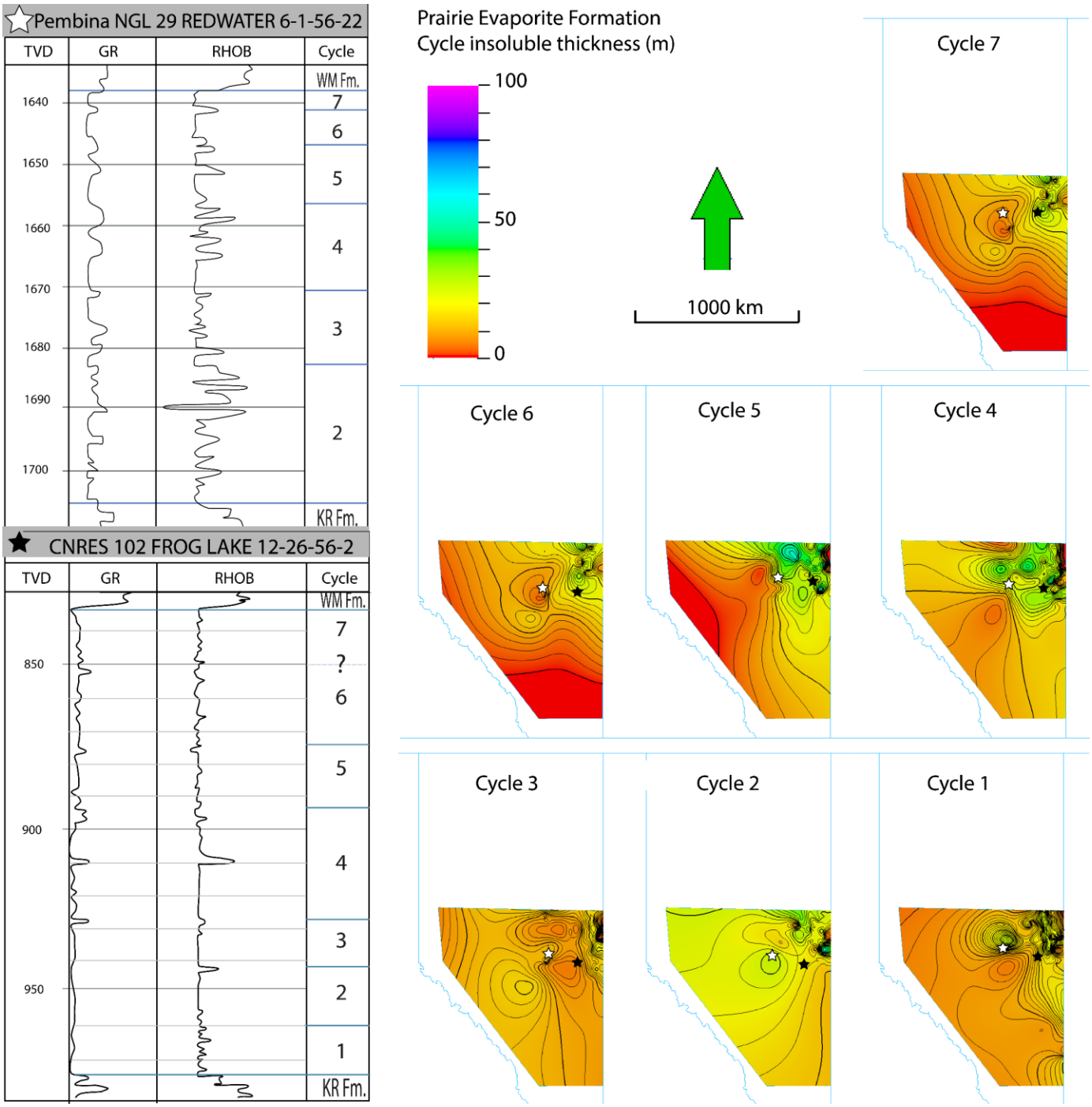


**Figure 14** Prairie Evaporite Formation cycle thicknesses within the study area. Two wells are indicated with stars in the plan-view maps, and their associated well log data are included. Cycles are described in Section 4.4. Abbreviations: KR = Keg River Formation, WM = Watt Mountain Formation. Raw data is available at https://doi.org/10.7939/DVN/LEXODD.

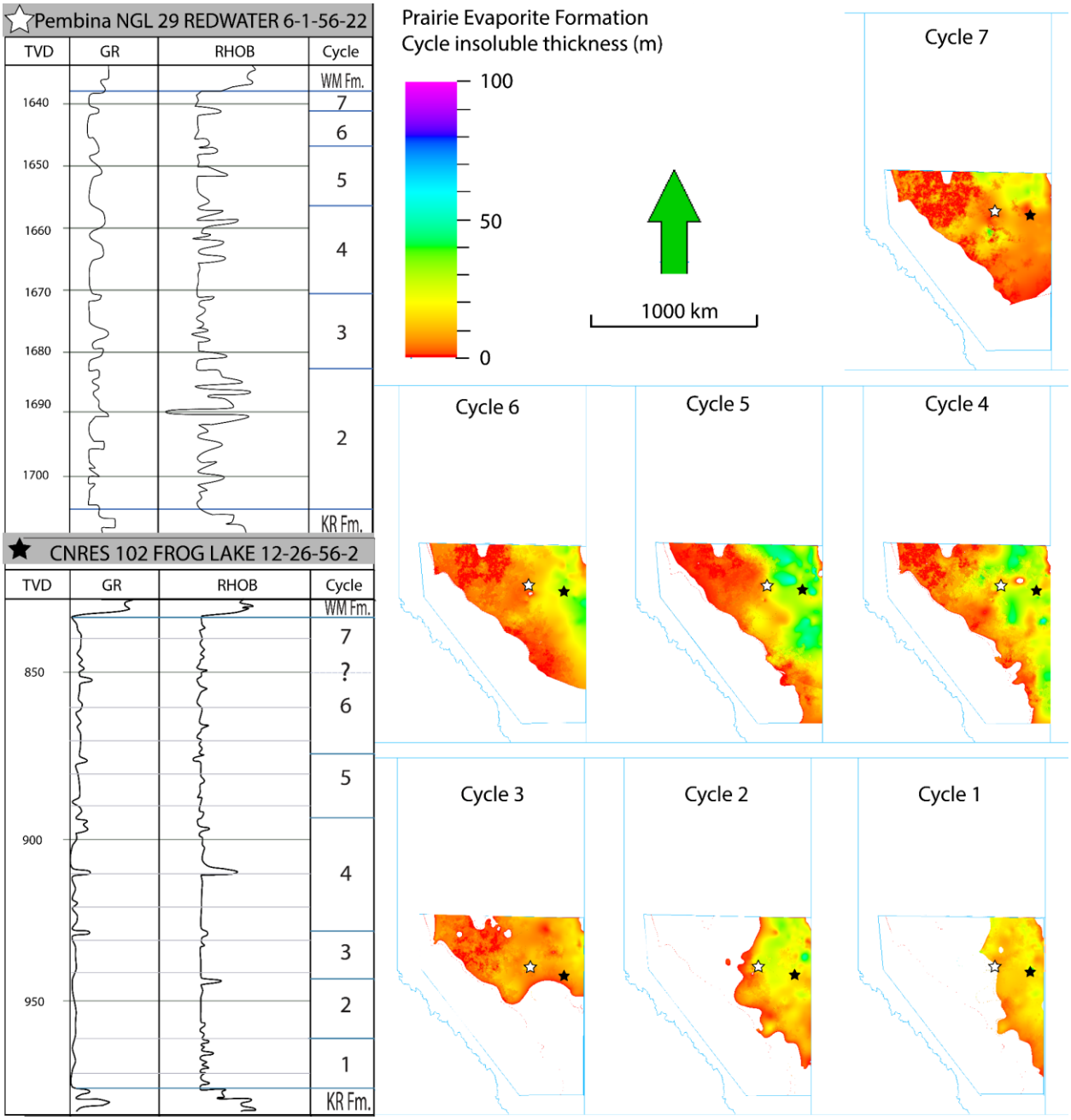


**Figure 15** Prairie Evaporite Formation cycle halite thicknesses within the study area. Two wells are indicated with stars in the plan-view maps, and their associated well log data are included. Cycles are described in Section 4.4. Abbreviations: KR = Keg River Formation, WM = Watt Mountain Formation. Raw data is available at https://doi.org/10.7939/DVN/LEXODD.

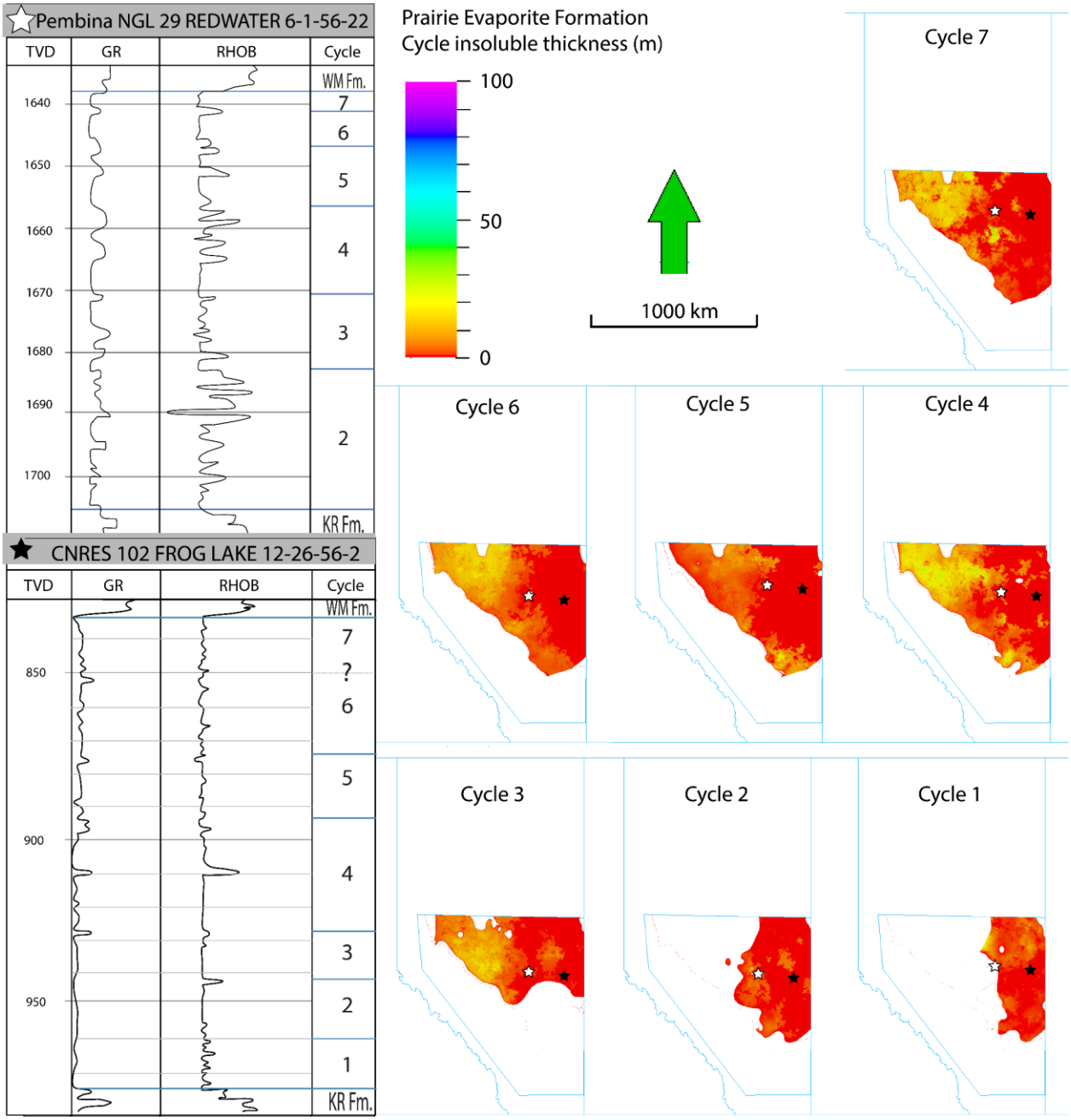


**Figure 16** Prairie Evaporite Formation cycle total insoluble thicknesses within the study area. Two wells are indicated with stars in the plan-view maps, and their associated well log data are included. Cycles are described in Section 4.4. Abbreviations: KR = Keg River Formation, WM = Watt Mountain Formation.First Cycle. Raw data is available at https://doi.org/10.7939/DVN/LEXODD.

Cycle One is the lowermost cycle, which is restricted to the northwest of the Central Alberta Basin and is the basal transition from the Keg River Formation dolomite into the anhydrite and marlstone beds of the Prairie Evaporite Formation (Figure 14 and Figure **16**). Cycle One is characterized by frequent thin beds of anhydrite interbedded with increasing thicknesses of halite upwards (Figure 17, Figure **18**, and Figure **19**).

### 4.4.1 Second Cycle

Cycle Two can be traced in well logs across the northern half of the Central Alberta Basin. The second cycle contains one bed of dolomite-cemented anhydrite with variable clay contents (Figure 18 and Figure **19**). In Core #1, the marker bed density peak correlates to a dark blue grey, bedded, dolomite cemented anhydrite.

### 4.4.2 Third Cycle

Cycle Three can be traced across the northern half of the Central Alberta Basin, preserved in Core #3 and #1. The cycle contains a single marker bed at the top of the cycle in well logs (Figure 18 and Figure **19**). The more southwestern of the cores (Well #1) contains a 20 cm thick massive beige anhydrite bed, whereas the northeastern core (Well #3) contains a 15 cm thick bed of haloturbated beige dolomitic anhydrite with lenses of halite (Table 1).

### 4.4.3 Fourth Cycle

Cycle Four is present across the Central Alberta Basin. At the top of the cycle, one distinct bed of mixed marlstone and anhydritic mudstone occurs; this bed divides into up to three beds to the east (Figure 18 and Figure **19**). The Muskeg 40 is a diagnostic gypsum marker bed (Hauck et al., 2017; Klingspor, 1969), and is considered a sub-cycle in the middle of this cycle, marked by a sharp decrease in sonic intensity from 95 μs/ft to 66 μs/ft. Where intersected by core from Well

#3 (Table 1), the one distinct marker bed density peaks in well logs correlate with a 4.5 m thick shaley siltstone without calcite.

#### 4.4.4 Fifth Cycle

Cycle Five is restricted to the northern part of the Central Alberta Basin and contains two anhydrite marker beds at the top of the unit less than 5 m (vertically) apart, which are considered as a single couplet due to variable facies across the basin (Figure 18 and Figure **19**). The log signature of Cycle Five marker beds is characterized by high density signal, allowing for differentiation between marker beds and halite with chaotic mud, which have a lower signal. Strong density peaks in well log correlate to a bed composed of marlstone in core from Well #3 (Table 1).

#### 4.4.5 Sixth Cycle

Cycle Six occurs above Cycle Five. Cycle 6 is identifiable within evaporite well logs to the northern part of the Central Alberta Basin. Cycle Six contains two anhydrite marker beds less than 5 m (vertically) apart that are considered a single couplet, similar to Cycle Five, between which there is an increase in clay abundance from background levels (~ 10 gAPI) to ~ 20 gAPI (Figure 16). In core from Well #3 (Table 1), the top marker bed is a dolomite-cemented mudstone in core. To the south, an increase in insoluble material and a shift away from halite facies obscures the individual marker beds in well logs. In the wells where both upper anhydrite beds are present, the uppermost anhydrite bed is used as the top of the cycle (Figure 18 and Figure **19**).

#### 4.4.6 Seventh Cycle

The uppermost cycle of the Prairie Evaporite Formation (Cycle Seven) terminates at a sharp contact with the overlying Watt Mountain Formation (Figure 17). Cycle Seven consists of

bedded halite, halite with chaotic mud, anhydritic mudstone, and sylvinite. The marker bed of this cycle terminates at the start of the overlying Watt Mountain Formation and is likely amalgamated with the mudstone of the Watt Mountain Formation in areas of truncation or dissolution of the Prairie Evaporite Formation halite. This cycle is thickest in the north-eastern corner of the Central Alberta Basin except where thinning occurs in the east (Figure 14). Core from Well #1 contains Cycle Seven's marlstone marker bed (Table 1). Core from Well # 3 contains the rock salt deposits of Cycle Seven (Table 1). These rock salts contain the most abundant sylvinite deposits of all other cycles in the study area.

# 5 Discussion

Spatial relationships of salt facies are typically described by correlation of vertical facies sequences as opposed to tracing lateral facies transitions. Research into lateral facies transitions has been hampered by quality, quantity, and accessibility of drill core as well as a lack of modern depositional analogues. Ancient salt giant deposits are modeled after modern environments such as sabkhas and playas, which are similar but not equivalent to ancient environments (Arthurton, 1973; Dean, 2014; Harraz, 2015; Kendall, 1978; Lowenstein, 1988; Lugli, 2009; Powers and Holt, 2007; Smoot and Lowenstein, 1991; Taj and Aref, 2015; John K. Warren, 2016). To further pursue regional evaporite correlation, I propose a scheme to recognize salt facies across large distances using well log signatures where core data is lacking (Section 4.2). This scheme is calibrated using core logs and compared against idealized playa depositional models (Kendall, 2010; Lowenstein and Hardie, 1985; Robertson, 1990; John K. Warren, 2016). Facies and depositional interpretations can then be compared against accepted models of ancient and modern evaporite environments for accuracy according to uniformitarianism. Evaporite depositional systems are unique in that they are defined by hydrologic regime and so the depositional environment must be inferred from the stage of evaporation within a concentrating-upwards cycle that each facies represents (John K. Warren, 2016). A three-dimensional basin model for the Prairie Evaporite is generated from the correlated cores and well logs in terms of evaporation cycles bounded by insoluble beds. Insoluble beds are easily recognized across the basin based on their characteristics in well logs (Table 3). They can be used to correlate cycle boundaries that I define as capping cycles that are tens of meters thick, and which occur in wells across the basin. Insoluble beds that are not laterally continuous over large distances, or are associated with cycles less than ten meters thick, are considered sub-cycle intra-unit insoluble layers.

### *5.1 Applicability of well log data for basin facies correlation*

Sparse core coverage limits effective basin correlation and interpretation; well logs are complementary tools alongside core logs, both preserving evidence of many sedimentary features of evaporite rocks (Brodylo and Spencer, 1987). Wire-line logs are particularly well-suited to interpreting bulk lithology and insoluble content in halite deposits due to the significant log signal differences between halite and insoluble material (Table 2) (Alger and Crain, 1966; Crain and Anderson, 1966). I compared 7 core logs (Table 1) and the respective wireline logs in the Central Alberta Basin to identify wireline features that correspond to facies seen in core (Figure 11 and Figure **12**; Appendix E). Interpretations of wire-line logs are validated by core facies descriptions (Figure 17, Appendix E). After calibration by this proposed method, two cores hundreds of kilometers apart can be confidently correlated (Figure 17).

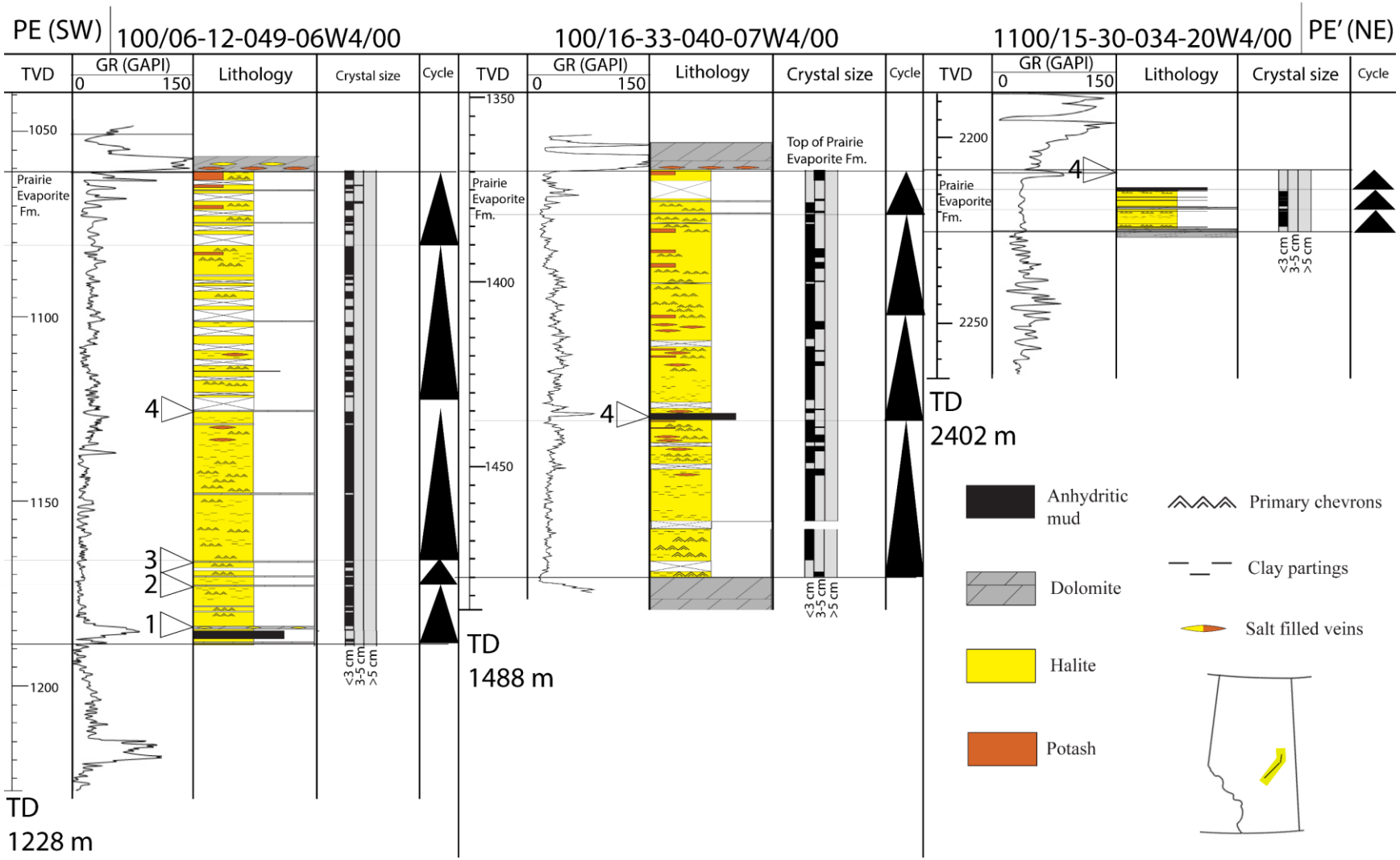


**Figure 17** PE-PE' core to well log correlation. Cycle marker beds are designated by empty triangles and a number corresponding to the cycle. The cycle column denotes evaporative sequences with respect to salinity, from least to most saline upwards.

This new proposed research methodology has allowed for facies (

Figure **20**) and to connect marker beds across the Central Alberta Basin. The Muskeg 40 bed is also identified across the northern Central Alberta Basin as the Cycle 4 sub-cycle gypsum bed (Brodylo and Spencer, 1987; Meijer Drees, 1994; Mossman et al., 1982; Rogers, 2017).

This method is not suitable for interpreting sedimentary fabrics that have not been calibrated to core, or for features with thinner than the resolution of the well log data.

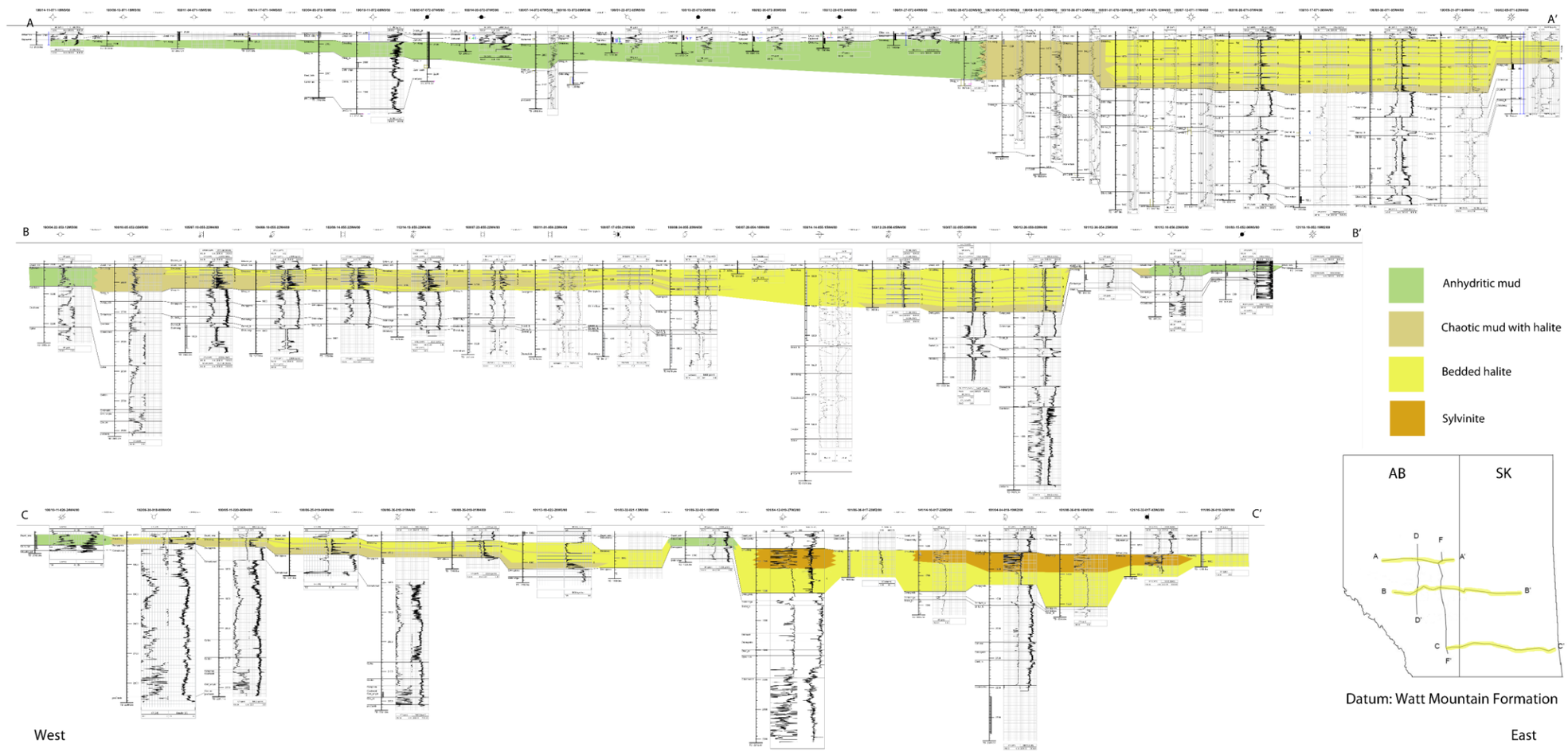


**Figure 18** East-west cross sections of the Prairie Evaporite Formation across the basin (locations shown on the inset map). Top) A-A' Middle) B-B' Bottom) C-C'. Enlarged photo available as plate 10. Raw data is available at https://doi.org/10.7939/DVN/LEXODD.

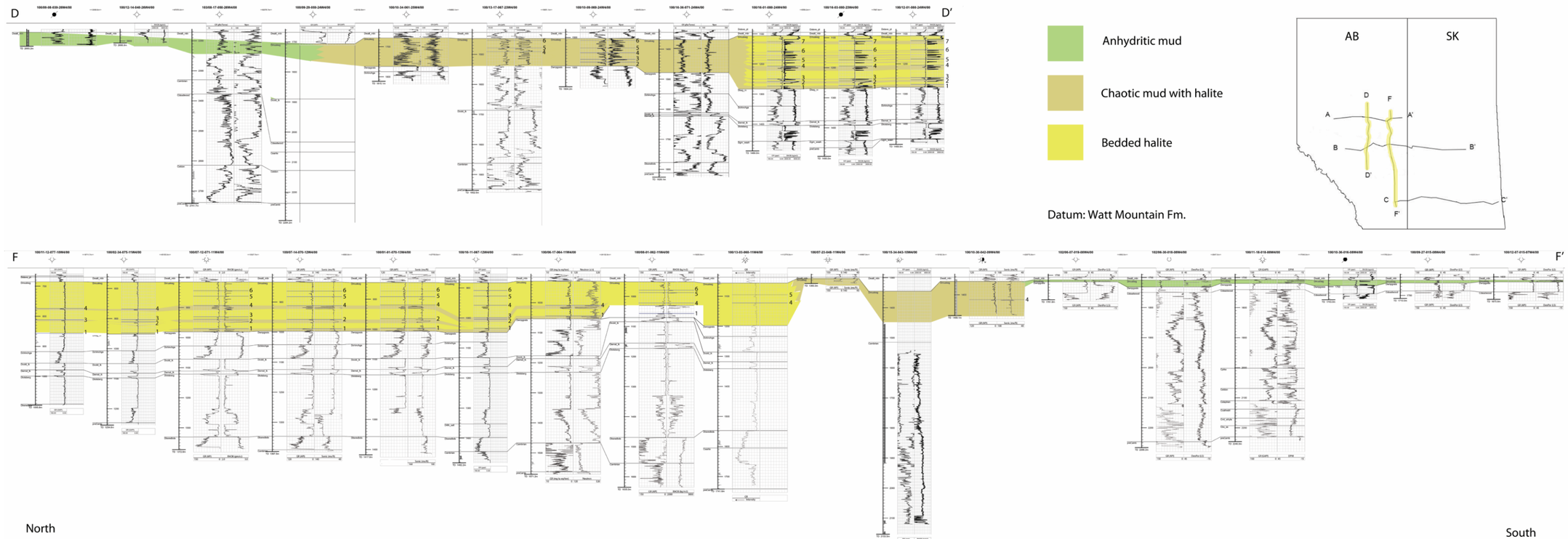


**Figure 19** North-south cross sections of the Prairie Evaporite Formation across the basin (locations shown on inset map). Top) D-D' Bottom) F-F'. Enlarged photo available as plate 11. Raw data is available at https://doi.org/10.7939/DVN/LEXODD.

Despite these limitations, distribution of evaporite facies can be mapped with more confidence over larger distances due to increased data density with the inclusion of wireline logs (Figure 18 and Figure **19**).

### *5.2 Depositional model of Prairie Evaporite Formation:*

Sea level and climate fluctuated during the Givetian, as a result of which the hydrology of the Central Alberta Basin cycled between net positive and net negative water input (Holter, 1969; Johnson et al., 1985; Wardlaw and Schwerdtner, 1966). Intermediate salinity deposits correspond with high sea level and humid climate versus hypersaline environments that correspond with water starvation and aridity. Each depositional environment corresponds to a set of facies, the distribution of which is controlled by climate, hydrology, and location in the Central Alberta Basin. Fluid chemistry exerts a strong control on evaporite mineral precipitation (carbonate, gypsum, and halite) during evaporative concentration and has been integral to expanding evaporite sedimentologic research (Hardie and Eugster, 1971; Jones, 1965; Smoot and Lowenstein, 1991). Vertical gradational contacts in the Prairie Evaporite Formation are interpreted to reflect deposition during gradual climate change, whereas sharp, disconformable contacts are considered to reflect deposition during events such as storms or floods. There are approximately 3-5 dissolution layers for every third of a meter, this is a minimum estimation due to removal of halite upon influx of low salinity water at the surface and after burial.

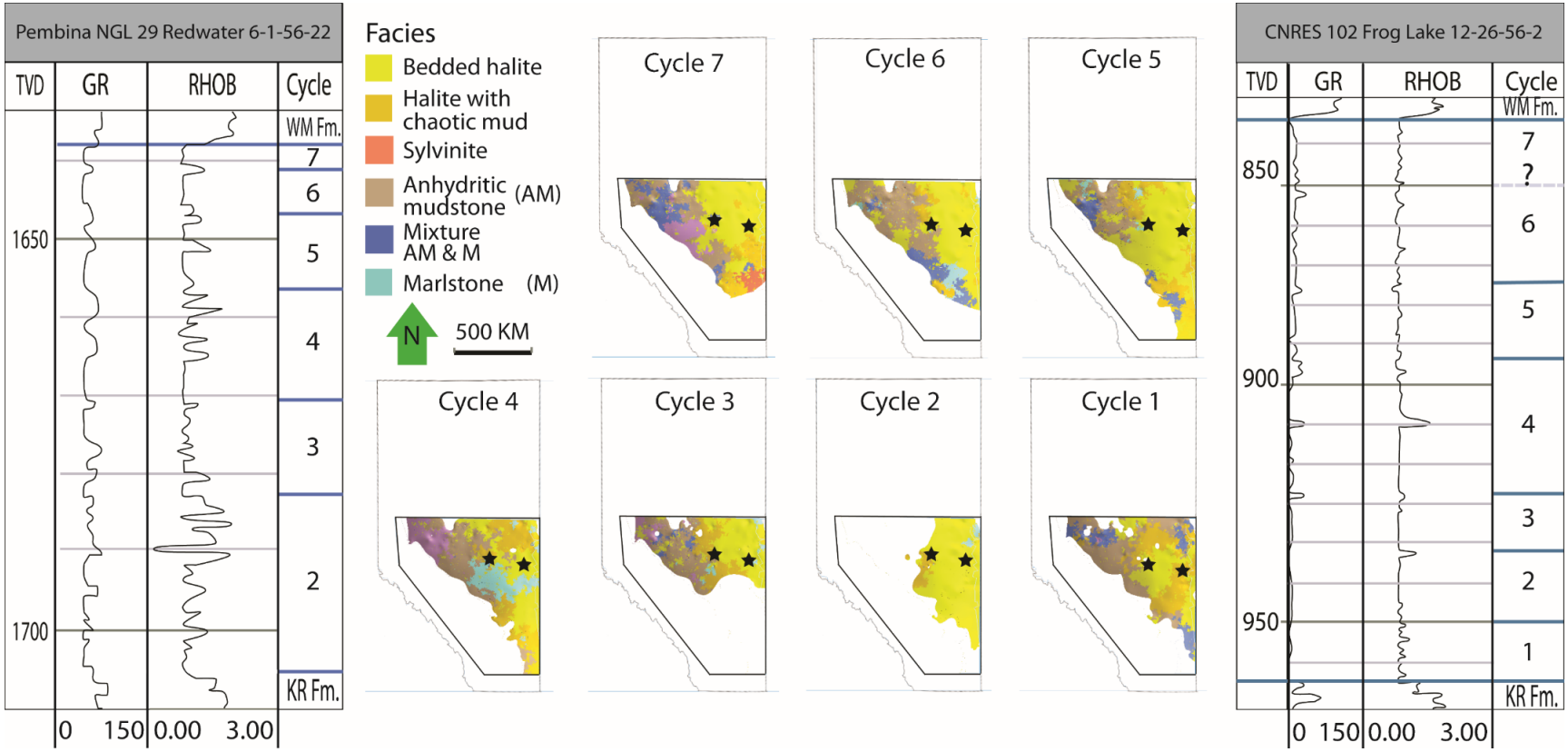


**Figure 20** Facies map of each cycle in the Prairie Evaporite Formation based on facies descriptions (Section 4.1). Cycles refer to Section 4.4. The question mark (?) indicates an approximate cycle top, based on surface modelling. Abbreviations: KR = Keg River Formation, WM = Watt Mountain Formation. Raw data is available at https://doi.org/10.7939/DVN/LEXODD.

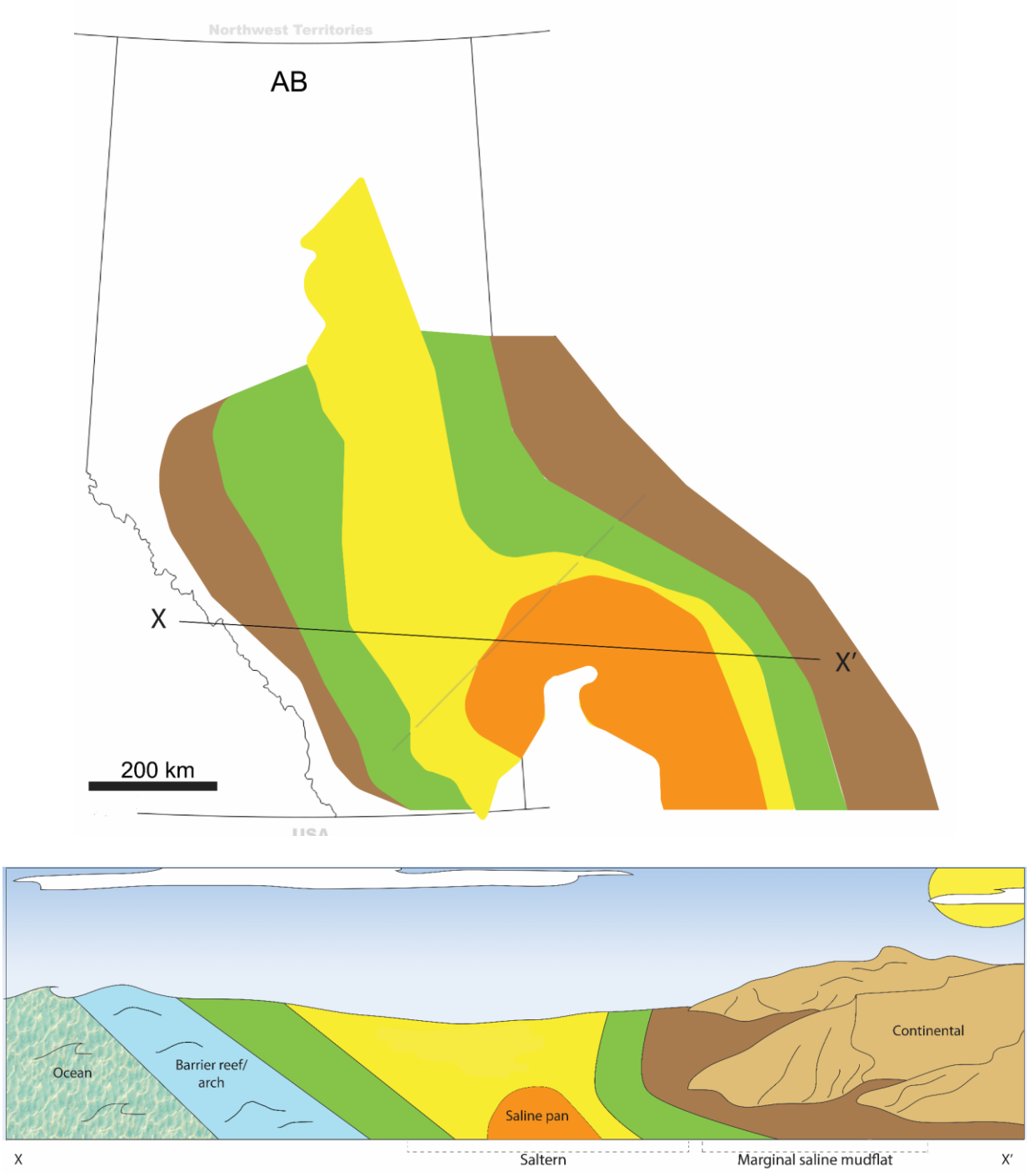


**Figure 21** Top: plan view map of Alberta and distribution of facies for the PE Fm. Indicated line (X-X') corresponds to schematic perspective drawing in the bottom figure based on Kendall (2010). Bottom: schematic perspective drawing of line X-X' showing one possible regional distribution of facies based on facies maps (

Freshening events likely initiated from the northwest of the Central Alberta Basin (Figure 3) based on a shift towards increasingly saline facies to the southeast (Figure 21; Klingspor, 1969; Wardlaw and Reinson, 1971; Warren, 2016). Nearshore low salinity facies to the west and south of the study area are marlstone and anhydritic mudstone, whereas eastern hyper-saline facies consist of halite with chaotic mud, bedded halite, and sylvinite (Figure 18, Figure **19**, and

**Figure 20**). Stratigraphic records are expected to be spatially variable and asynchronous due to hiatuses in deposition, or erosion of existing stratigraphy (Lowenstein et al., 2003).

Facies transition from marlstone in the far western Central Alberta Basin to potash in the far eastern CAB (Figure **17**, **Figure 18**, and

**Figure 20**) and from halite with chaotic mud in northern CAB through bedded halite to chaotic mud with halite to anhydrite towards southern CAB on a NW cross section (Figure 19 and

**Figure 20**). Deep water environments have been excluded from consideration due to overwhelming evidence of a shallow (< 10 m) maximum brine depth such as thin bedded halite beds, which requires frequent salinity changes unlikely to occur in more stable deeper waters, as well as lack of deep features such as laminate halite beds and debris flows (Kendall, 2010; McTavish and Vigrass, 1987; Wardlaw and Schwerdtner, 1966). Prairie Evaporite Formation facies are grouped into the saltern, saline pan, and marginal saline mudflat facies associations and compared with ancient and modern depositional environments to deduce ancient depositional environments (Figure 22).

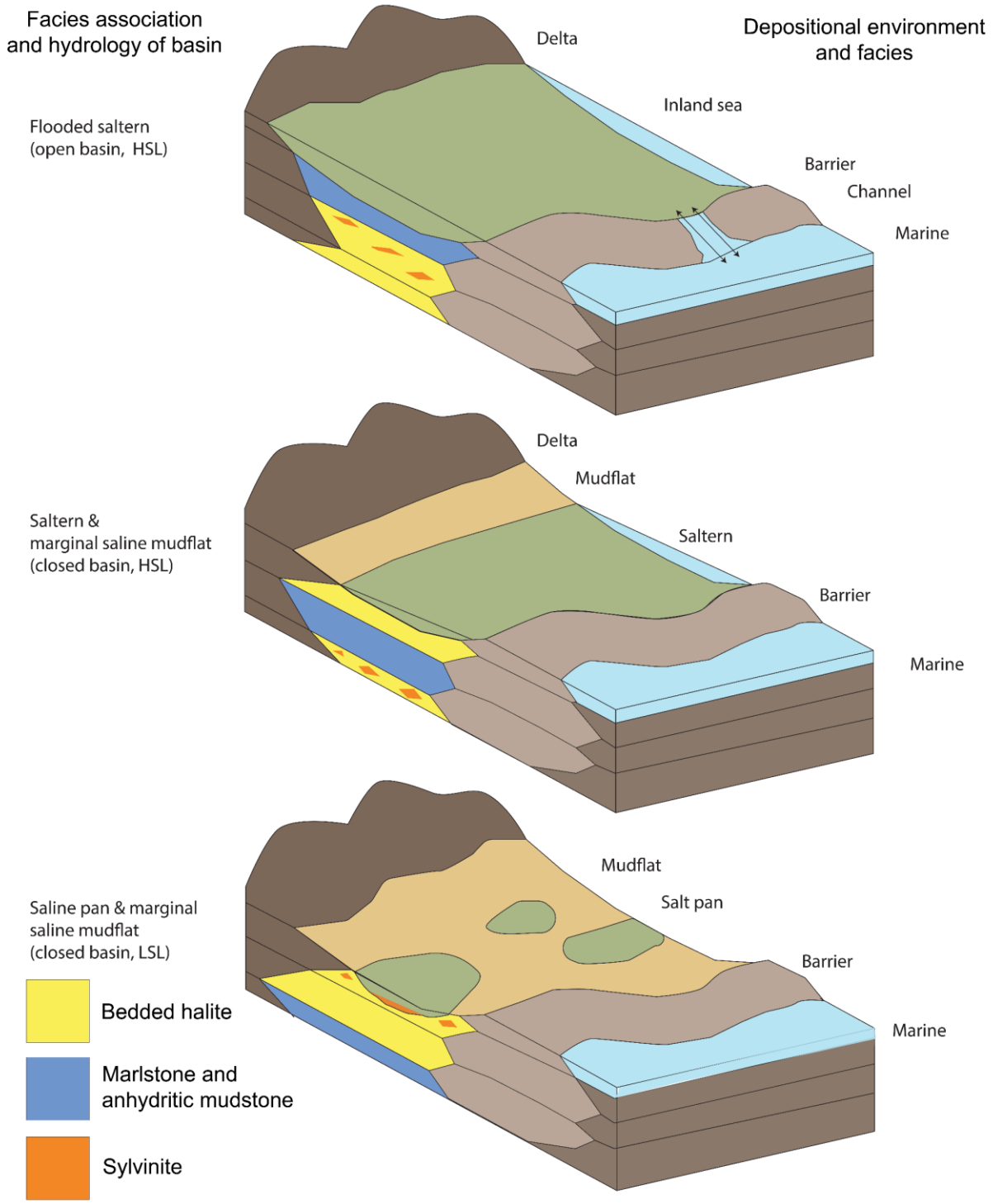


**Figure 22** Spatial relationship of facies deposition and hypothesized depositional environment for each facies association in the Prairie Evaporite Formation. HSL – high inland sea level, LSL – low inland sea level.

### 5.2.1 Saltern (subaqueous evaporite seaway)

The saltern facies association is defined by bedded halite and marlstone-anhydritic mudstone laminae couplets. Saltern deposits are composed of shoaling-upward beds (parasequences) from thin low-salinity beds at the base (i.e., dolostone, anhydrite) upward to thick halite beds with low insoluble contents (John K Warren, 2016). Bedded halite conformably overlies and unconformably underlies anhydritic mudstone or marlstone. Bedded halite deposits are the most voluminous facies constituting 46 % of the Prairie Evaporite Formation bulk volume, and represent hyper saline conditions (~ 90 % seawater evaporated; Bąbel and Schreiber, 2014). Common sedimentary features of salterns include dissolution beds (**Plate 5**), chevron halite (Plate 2), diagenetic spar (**Plate 9**), and laminated couplets of anhydrite and marlstone (**Plate 3**).

The Ordovician-Silurian Mallowa Salt (Cathro et al., 1992; John K. Warren, 2016), and modern shallow coastal evaporitic playas such as the Hutt Lagoon, Western Australia (Arakel, 1988, 1980) are examples of saltern deposits. Bedded halite is observed in core of the Prairie Evaporite Formation with chevron fabrics (Plate 2) and associated mud drapes (Plate 3) that are comparable to fabrics interpreted by Cathro et al. (1992) as shallow (< 10 m deep) subaqueous deposits in the Mallowa Salt. These same features are currently being deposited in the Hutt Lagoon in shallow ephemeral saline ponds. Mud drapes within these deposits occur at small scales that cannot be correlated between wells. Such small scale drape features may suggest a rough sea floor surface and the accumulation of insolubles in mini-basins (John K Warren, 2016). Laminated anhydritic mudstone and marlstone are a minor component of the Prairie Evaporite Formation, but are interpreted as the result of freshened water influx similar to that of the Hutt Lagoon (Arakel, 1980; Hardie and Eugster, 1971; Wardlaw and Schwerdtner, 1966).

Saltern deposits are found in between the Elk Point Basin edge and center (Figure 21,

**Figure 20**, and Figure **22**). The vertical and lateral transition from anhydritic mudstone or marlstone to bedded halite tends to be sharp and conformable owing to precipitation via variation in salinity. As fluid is reintroduced to the basin, bedded halite is dissolved and anhydritic mudstone/marlstone is deposited on top of the new dissolution surface (Plate 5 and Plate **7**). Following this flooding and dissolution, a bed of halite with chaotic mud is deposited, and subsequent beds of halite follow with decreasing concentrations of insoluble material. Bedded halite deposits can reach tens of meters in thickness, consisting of individual beds < 0.3 m thick. Insoluble material is thickest in the western Central Alberta Basin. Conversely, bedded halite comprises an increasing proportion of the facies association in the eastern Central Alberta Basin.

During the Middle Devonian, the Central Alberta Basin was isolated from constant communication with the open ocean by emergent topography. Isolation of a basin, punctuated by flooding of seawater, combined with high evaporation rates produces a shallow body of water with a relatively high salinity. In general, shallow bodies of water are more susceptible to changes in salinity due to influx of low-salinity fluid. Influx of lower salinity water when mixed with small volumes of concentrated brine dissolves the evaporite sediment, resulting in bedded halite bounded by layers of marlstone and anhydritic mudstone. Thick beds of anhydrite and marlstone are associated with major freshening events. Based on these observations, I infer that the saltern facies association was deposited in a standing body of shallow water in an inland continental basin which was affected by periodic freshening events.

### 5.2.2 Saline Pan

The saline pan facies association includes halite with chaotic mud, sylvinite, and clear coarse halite. Characteristic sedimentary features of the saline pan facies association include pipes filled with coarse clear halite, vugs lined with chevron halite, and displacive halite cubes in mud

(Lowenstein and Hardie, 1985). Saline pan deposits constitute only ~ 2 % of the Prairie Evaporite Formation in the Central Alberta Basin.

Saline pan deposits are present in the Saskatchewan Prairie Evaporite Formation (Holter, 1969; Worsley and Fuzesy, 1979), Permian Salado Formation (Casas and Lowenstein, 1989; Lowenstein, 1987, 1988), and modern day Death Valley, California, USA deposits (Lowenstein et al., 1999; Lowenstein and Risacher, 2009). Sylvinite crosscut with centimeter- to meter-scale vugs (salt horses; Broughton (2019)) and networks of pipes are reported by underground mining operations of the Prairie Evaporite Formation in Saskatchewan (John K Warren, 2016). These features are comparable to centimeter-scale pipe and vug fabrics observed in core studied for this project (Plate 5). Saline pan deposits of the Permian Salado Formation contain irregular, discontinuous lenses of silty mud trapped in vugs (Lowenstein 85), similar to the sub-cycle beds of anhydritic mud documented in Prairie Evaporite saline pan deposits (Figure 18 and Figure **19**). Lenses of mud in the Salado Formation are interpreted by Bobst et al. (2001) to result from surface exposure and dissolution of the soluble matrix by rain. This is a plausible interpretation of the anhydritic mudstone layers within the Prairie Evaporite Formation saline pan deposits. Similar processes of dissolution occur in Death Valley, USA, a desiccated saline pan in which concentrated brines occur within 1 m of the surface (Lowenstein et al., 1999; Lowenstein and Risacher, 2009), where introduction of low salinity water to desiccated sediments produces dissolution pipes and vugs similar to that of the Salado formation and the Prairie Evaporite Formation. Desiccation of Death Valley sediments and subsequent displacive evaporite growth also creates meter-scale polygons due to buckling. These polygons trap discontinuous, lenticular bedding of mud similar to discontinuous lenses of mud seen in cross sections of the Prairie Evaporite Formation (Figure 18 and Figure **19**; Lowenstein & Hardie (1985), Lowenstein et al. (1999))

Sylvinite beds, which characterize saline pan deposits, are typically < 0.5 m thick and reach maximum thicknesses of 1.25 m in studied core (Figure 11). Saline pan deposits are only found in the south-eastern most corner of the Central Alberta Basin (Figure 18C). Vertically, sylvinite is found at the top of evaporative sequences (**Error! Reference source not found.**). Saline pan deposits conformably overlie saltern deposits and conformably underlie saline mudflat deposits. In the event of a flood during saline pan deposition, the evaporative sequence is restarted. In this event, saline pan deposits unconformably underlie saltern deposits, though preservation of sylvinite is unlikely due to the soluble nature of K and Mg salts. Sylvinite deposits are not reported in the lower half of the Prairie Evaporite Formation, but beds containing sylvinite become more frequent and thicker towards the top of the formation, indicating a brining-upward trend from Cycle One through Cycle Seven.

The occurrence of sylvinite facies requires extreme concentrations of Mg and K, achieved by evaporation of brine. Sylvinite was deposited in the innermost Central Alberta Basin due to the tendency of concentrated brines to pool in the lowest topographic points (Braitsch, 1971; Broughton, 2019). Dissolution textures such as the vugs and pipes occurring in Prairie Evaporite Formation saline pan deposits are associated with very shallow brine depths and even temporary (i.e., seasonal) dryness as seen in the Salado Formation and modern Death Valley sediments (Lowenstein, 1988; Lowenstein et al., 1999; Lowenstein and Hardie, 1985). Sylvinite facies can only be deposited in end-member inland ponds, and is highly susceptible to dissolution and alteration (Broughton, 2019; Guilbert and Park, 1986). Lenses of mud seen in cross sections A-A', B-B', C-C', D-D', and F-F' (Figure 18 and Figure **19**) could indicate topographic lows that trap sediment between buckle ridges as has been documented in Death Valley (Lowenstein et al., 1999; Lowenstein and Hardie, 1985). Therefore, Prairie Evaporite Formation saline pan sediments

are inferred to be deposited in a nearly dry basin dominated by diagenetic growth in the subsurface and characterized by deposition of potash from concentrated brine.

### 5.2.3 Marginal saline mudflat

The marginal saline mudflat facies association includes halite with chaotic mud, marlstone, and anhydritic mudstone, and comprises ~ 6% of the Prairie Evaporite Formation. Features characteristic of marginal saline mudflat deposits are mud cracks, teepee structures, fibrous sylvinite, massive mud beds, and localized lenses of displacive evaporites (Powers and Holt, 2007).

Marginal saline mudflat deposits occur in the Saskatchewan Prairie Evaporite Formation, the Permian Rustler Formation (Powers and Holt, 2007), and the modern Salar de Atacama (Bobst et al., 2001; Lowenstein et al., 2003). Prominent mud cracks occur in the saline mudflat beds of the upper Prairie Evaporite Formation, unearthed during underground mining operations in Saskatchewan (Mossman et al., 1982). These beds of mud are correlated with Cycle Six and Cycle Seven in the Central Alberta Basin (Figure 18 and Figure **19**), and consist of dolomite, anhydrite, clay, and variable amounts of quartz silt. Similar beds within the Permian Rustler Formation are described by Powers and Holt (2007), in which layers of mudstone contain displacive halite and are overlain by brecciated anhydrite. Powers and Holt (2007) interpret the displacive halite to be syn-depositional, and the brecciation of anhydrite to be caused by removal of underlying halite. Displacive cumulate halite beds (Plate 4) and brecciated mudstone beds associated with exposure (Plate 7) are both noted in massively bedded mudstone in the studied cores. Such massive beds of anhydrite-dolomite-clay in the Salar de Atacama are interpreted as in-situ deposits caused by capillary evaporation under exposed arid settings (Bobst et al., 2001).

Marginal saline mudflat deposits are found throughout the Central Alberta Basin, but are dominant to the west and south-west near the Peace Ricer Arch and Western Alberta Ridge (Figure 21,

**Figure 20**, and

**Figure 20**). Vertically, marginal saline mudflats are found on top of an erosive boundary due to exposure of an evaporative deposit, or intercalated with siliciclastic deposits from erosion of emergent topography (John K. Warren, 2016). Marginal saline mudflat deposits comprise the majority of insoluble material within the Prairie Evaporite Formation, and so the extent of the mudflat facies is mappable by the total thickness of insoluble material (Figure 16). Marginal saline mudflats deposits are thickest in the western Central Alberta Basin and thin to the east, where mudflat beds interfinger with hyper-saline (saltern and salt pan) deposits. These beds are typically overlain by marlstone and anhydritic mudstone and are indistinguishable from said overlying beds on well logs. Due to the difficulty of distinguishing lithologic changes between mudstone, marlstone, and anhydritic mud, I hypothesize that marginal saline mudflat deposits are continuous beyond the halite margins but cannot be identified using the scheme proposed in this project.

Marginal saline mudflats bordered the epeiric sea as extensive flats of fine-grained sediment. During periods of severe desiccation, massively-bedded silty mud was deposited in the marginal saline mudflat over saltern and salt pan deposits. A combination of insoluble mapping, correlation of core logs, and analysis of mineral composition indicates a trend of thick marginal marlstone beds in the western Central Alberta Basin that transition into thinner anhydritic mud beds to the east. No teepee structures are observed in marginal saline mudflat deposits seen in Prairie Evaporite Formation cores studied for this research. This lack of teepee structures has been interpreted to indicate a basin floor that never experienced prolonged dry periods (Jin and

Bergman, 1999; Klingspor, 1969). Mud deposits are cross-cut by veins of fibrous sylvite, which bear a strong resemblance to mud cracks (Plates 7 and 8). These veins are interpreted as concentrated brine that sank and precipitated in porous sediment. Due to the presence of fibrous sylvite veins in mudstone, it is apparent that the Central Alberta Basin experienced prolonged (i.e., years) dry periods. Therefore, either teepee structures never formed or, the lack of teepee structures may be due to erosion. The presence of brecciation in mudstone supports the latter.

### *5.3 Water input and cyclicity in the basin:*

Water cyclicity (i.e., water depth and chemistry) is influenced by sea level, climate change, and seasonal variation (Kendall, 1978). Kendall (1988) states that "there is no more important variable than the type of brine and its origin,'' as a control on evaporite deposition. With decreasing salinity insoluble sediments such as clastics, carbonates, and anhydrite are preferentially produced and preserved. Basin water salinity is based on the ratio of low salinity water influx (Δ input) to evaporation rate (Bąbel and Schreiber, 2014; Braitsch, 1971; Kendall, 1978). During events of large water influx, such as sheet floods or tropical storms, salts are dissolved leaving a layer of concentrated insolubles from between and within the dissolved deposit on top of an erosional surface. After dissolution and the onset of evaporation, the normal evaporative sequence starts. If water influx and evaporation rates are slow, a delicate balance between salt precipitation and non-deposition occurs. If water influx is less than evaporation, end member deposits such as potash are deposited and an exposure surface is created (Kendall, 2010; Lowenstein and Hardie, 1985; Lugli, 2009; John K. Warren, 2016). The range of mineral deposits is limited by the source of water and brine composition.

The Devonian Elk Point Group evaporites were deposited from a $CaCl_2$ brine (Spencer, 1987) and followed the calcite, gypsum, halite, sylvite, carnallite evaporative sequence (Braitsch, 1971) that can be traced both vertically and laterally across the study area. Carnallite found in Saskatchewan does not follow this trend, but is hypothesized to be a diagenetic alteration of sylvite after introduction to magnesium rich brine (). Studies of other Devonian deposits across the Western Canada Sedimentary Basin record water depth profiles in non-evaporitic deposits, which can be compared against evaporative facies. Johnson and Murphy (1984), Johnson et al. (1985), and Rogers (2017) each report transgressive-regressive cycles within and surrounding the Central Alberta Basin. All marker beds defined in this research fall were deposited both during transgressive and regressive events reported by Rogers (2017) and Johnson et al. (1985). This discordance with sea level is due to the restrictive nature of the environment and limited communication between the sea and basin (Lugli, 2009). Sea level is therefore interpreted as only a minor force on hydrologic change in the Central Alberta Basin.

Despite the difficulty in "untangling" the numerous influences that produce climatic changes, evaporite basins are known for "amplifying" climate records (Stein, 2001): significant changes in environment or climate are often reflected in facies variations in basins. During particularly humid periods, evaporites are deposited at a relatively slower pace due to large volumes of low salinity water influx from continental sources and suppressed evaporation. Deposits formed during periods of high humidity are dominated by bedded halite and halite with chaotic mud, with vertically-oriented chevron crystals. Often interspersed throughout these humid deposits are thin couplets of anhydritic mud and marlstone associated with low salinity water flooding in a saltern environment. This is opposed to arid eras that favour evaporite precipitation in salterns and salt pans. Arid deposits are dominated by bedded halite, halite with chaotic mud, and sylvinite. Characteristic

features of deposits of an arid environment are pipes, vugs, and mud cracks. The base of the Prairie Evaporite Formation is represented by Cycle One, which is composed of halite with chaotic mud frequently interbedded with anhydritic mud and marlstone beds, inferred to have been deposited in a humid environment. The top of the Prairie Evaporite Formation is represented by Cycle Seven, which is inferred to have been deposited in an arid environment. The ratio of halite to insolubles increases vertically within individual cycles, which is interpreted to represent increasing salinity over time. This same trend (e.g., increasingly saline) is also observed in successive cycles, as Cycle one contains more halite and insoluble material relative to Cycle Seven, which in turn contains more sylvinite. Overall, Middle Devonian climate became increasingly arid between the time of deposition of the Keg River and Watt Mountain Formations in the Central Alberta Basin. During relatively humid periods, insoluble beds were deposited mainly in northern Central Alberta Basin (Figure 16), which corresponds with an increase in water influx. The large volume of water needed to deposit thick insoluble beds indicates that spill-over, rather than slow seepage through the Presqu'ile barrier, may have been the primary cause of marker bed deposition. Insoluble thickness is thickest in the northwest Central Alberta Basin near the Peace River Arch, but within Cycles One, Two, Four, and Five, $\geq$ 10 m thick insoluble layers also extend into the southern Central Alberta Basin (Figure 16). The occurrence of thick insoluble layers in the southern Central Alberta Basin is apparent based on an increased abundance of clastics that interfinger with halite in core from Well #4 in the southwest Central Alberta Basin (Table 1). This suggests that the layers were deposited by a water and silicate source coming from the southwest of the Central Alberta Basin, consistent with the hypothesis of a structural barrier in southwest Alberta through which water occasionally flowed (Williams 1984)

# 6 Summary and Conclusions

In this study I analyzed wireline logs from 994 wells and logged seven cores from the Central Alberta Basin. The focus of this analysis was to assess stratigraphic relationships, textural features, and depositional environment of the Middle-Devonian Prairie Evaporite Formation. Based on this study I have characterized six evaporite facies which can be identified in core and in wireline logs. Seven facies cycles within the Prairie Evaporite Formation of the Central Alberta Basin are defined. These facies are mapped across the Central Alberta Basin to determine the spatial organization of depositional environments.

Drill core preserving the salt beds of the Elk Point Group in Alberta are scattered, distant, and incomplete. Therefore, I propose a scheme that correlates facies logged in available core with data in wireline well logs, which are much more widely available (Table 3). Cycles of evaporite deposition are present in the studied cores, and include brackish anhydritic mudstone, marlstone, hypersaline bedded halite with growth aligned chevron fabrics, desiccated pan chaotic muddy halite, sylvinite, and coarse clear halite in pipes and vugs (Figure 17). These facies associations are predictable and agree with epeiric sea models. I define seven facies cycles within the Prairie Evaporite Formation across the Central Alberta Basin (Section 4.4). Within each cycle, deposition of each facies association is modeled across the basin (Figure 18 and Figure **19**). Each modeled facies is inferred to indicate deposition in a saline mudflat in the western Central Alberta Basin, a saltern environment in the eastern Central Alberta Basin, and a small region of saline pan environment in the extreme southeast Central Alberta Basin (

Figure **20**). This association is inferred to indicate that deposition in the west and southwest Central Alberta Basin was primarily in a nearshore environment, and an increasingly shallow and concentrated epeiric sea basinward (Figure 21 and

**Figure 20**).

Well log to core log facies-correlation may also be applied to other formations within the Elk Point Group such as the Cold Lake Formation and other evaporite deposits of the world, but first requires that core and wireline logs are correlated properly, and that the logs have sufficient resolution to identify small-scale features that may be marker beds. For example, this method could be applied to identification of facies within the Lotsberg Formation in the Central Alberta Basin.

## References


Alger, R.P.P., Crain, E.R.R., 1966. Defining evaporite deposits with electrical well logs, in: Second Symposium on Salt. The Northern Ohio Geological Society, Inc. pp. 116–130.

Andrichuk, J.M., 1951. Regional Stratigraphic Analysis of Devonian System in Wyoming, Montana, Southern Saskatchewan, and Alberta. Am. Assoc. Pet. Geol. Bull. 35, 2368–2408.

Arakel, A. V, 1988. Modern halite sedimentation processes and depositional environments, Hutt Lagoon, Western Australia. Geodin. Acta 2, 169–184. https://doi.org/10.1080/09853111.1988.11105165

Arakel, A. V, 1980. Genesis and diagenesis of Holocene evaporitic sediments in Hutt and Leeman lagoons, Western Australia. J. Sediment. Res. 50, 1305–1326. https://doi.org/10.1306/212F7BDF-2B24-11D7-8648000102C1865D

Arthurton, R.S., 1973. Experimentally produced halite compared with Triassic layered halite-rock from Cheshire, England. Sedimentology 20, 145–160. https://doi.org/10.1111/j.1365-3091.1973.tb01611.x

Bąbel, M., Schreiber, B.C., 2014. 9.17-Geochemistry of evaporites and evolution of seawater. Treatise on geochemistry 9, 483–560. https://doi.org/10.1016/B978-0-08-095975-7.00718-X

Bebout, D.G., Maiklem, W.R., 1973. Ancient anhydrite facies and environments, Middle Devonian Elk Point Basin, Alberta. Bull. Can. Pet. Geol. 21, 287–343.

Bobst, A.L., Lowenstein, T.K., Jordan, T.E., Godfrey, L. V., Ku, T.L., Luo, S., 2001. A 106 ka paleoclimate record from drill core of the Salar de Atacama, northern Chile. Palaeogeogr. Palaeoclimatol. Palaeoecol. 173, 21–42. https://doi.org/10.1016/S0031-0182(01)00308-X

Borchert, H., 1969. Principles of Oceanic Salt Deposition and Metamorphism. Geol. Soc. Am. Bull. 80, 821–864. https://doi.org/10.1017/CBO9781107415324.004

Braitsch, O., 1971. Salt Deposits Their Origin and Composition, in: von Engelhardt, W., Roy, R., Wyllie, P.J., Winchester, J.W., Hahn, T. (Eds.), Minerals , Rocks and Inorganice Materials. Springer, Berlin, Heidelberg, pp. 1–289. https://doi.org/10.1007/978-3-642-65083-3

Brodylo, L.A., Spencer, R.J., 1987. Depositional environment of the middle devonian telegraph salts, Alberta, Canada. Bull. Can. Pet. Geol. 35, 186–196.

Broughton, P.L., 2019. Economic geology of southern Saskatchewan potash mines Saskatoon. Ore Geol. Rev. 113, 103117. https://doi.org/10.1016/j.oregeorev.2019.103117

Broughton, P.L., 2013. Devonian salt dissolution-collapse breccias flooring the Cretaceous Athabasca oil sands deposit and development of lower McMurray Formation sinkholes, northern Alberta Basin, Western Canada. Sediment. Geol. 283, 57–82. https://doi.org/10.1016/j.sedgeo.2012.11.004

Burrowes, O.G., Krause, F.F., 1987. Overview of the Devonian system: subsurface of Western Canada Basin. Devonian Lithofacies Reserv. Styles Alberta 1–20.

Cant, D.J., 1988. Regional Structure and Development of the Peace River Arch, Alberta: A Paleozoic Failed-Rift System? CSPG Bull. 36, 284–295.

Casas, E., Lowenstein, T.K., 1989. Diagenesis of saline pan halite: comparison of petrographic features of modern, Quaternary and Permian halites. J. Sediment. Res. 59, 724–739. https://doi.org/10.1306/212F905C-2B24-11D7-8648000102C1865D

Cathro, D.L., Warren, J.K., Williams, G.E., 1992. Halite saltern in the Canning Basin, Western Australia: a sedimentological analysis of drill core from the Ordovician-Silurian Mallowa

Salt. Sedimentology 39, 983–1002. https://doi.org/10.1111/j.1365-3091.1992.tb01992.x
Cocks, L.R.M., Torsvik, T.H., 2011. The Palaeozoic geography of Laurentia and western Laurussia: a stable craton with mobile margins. Earth-Science Rev. 106, 1–51. https://doi.org/10.1016/j.earscirev.2011.01.007
Crain, E.R., Anderson, W.B., 1966. Quantitative Log Evaluation of the Prairie Evaporite Formation in Saskatchewan. J. Can. Pet. Technol. 5, 145–152. https://doi.org/10.2118/66-03-06
Dean, W.E., 2014. Marine Evaporites, in: Encylopedia of Marine Geosciences. Springer Science & Business Media, Dordrecht, pp. 1–10. https://doi.org/10.1007/978-94-007-6644-0_188-1
Domeier, M., Torsvik, T.H., 2014. Plate tectonics in the late Paleozoic. Geosci. Front. 5, 303–350. https://doi.org/10.1016/J.GSF.2014.01.002
Grobe, M., 2000. Distribution and Thickness of salt within the Devonian Elk Point group, western Canada sedimentary basin. Earth Sci. Rep. 2, 1–12.
Guilbert, J.M., Park, C.F., 1986. The Geology of Ore Deposits. W. H.
Gussow, W.C., 1957. Cambrian and PreCambrian geology of Southern Alberta.
Hardie, L.A., Eugster, H.P., 1971. The Depositional Environment of Marine Evaporites: a Case for Shallow, Clastic Accumulation. Sedimentology 16, 187–220. https://doi.org/10.1111/j.1365-3091.1971.tb00228.x
Harraz, H.Z., 2015. Evaporite Salt Deposits. https://doi.org/10.13140/RG.2.1.3231.3203
Hauck, T., Peterson, J.T., Hathaway, B., Grobe, M., MacCormack, K., 2017. New insights from regional-scale mapping and modelling of the Paleozoic succession in northeast Alberta: Paleogeography, evaporite dissolution, and controls on Cretaceous depositional patterns on the sub-Cretaceous unconformity. Bull. Can. Pet. Geol. 65, 87–114. https://doi.org/10.2113/gscpgbull.65.1.87
Hauck, T.E., Peterson, J.T., Hathaway, B., Grobe, M., MacCormack, K., Hathway, B., Grobe, M., MacCormack, K., 2017. New insights from regional-scale mapping and modelling of the Paleozoic succession in northeast Alberta: Paleogeography, evaporite dissolution, and controls on Cretaceous depositional patterns on the sub-Cretaceous unconformity. Bull. Can. Pet. Geol. 65, 87–114. https://doi.org/10.2113/gscpgbull.65.1.87
Holter, M.E., 1969. The Middle Devonian Prairie Evaporite of Saskatchewan, Saskatchewan Department of Mineral Resources, Report no. 123. Regina: Lawrence Amon, Queen's Printer.
Hsü, K.J., 1972. Origin of saline giants: A critical review after the discovery of the Mediterranean Evaporite. Earth-Science Rev. 8, 371–396. https://doi.org/https://doi.org/10.1016/0012-8252(72)90062-1
Jin, J., Bergman, K.M., 1999. Sequence stratigraphy of the Middle Devonian Winnipegosis carbonate-prairie evaporite transition, southern Elk Point Basin. Carbonates and Evaporites 14, 64–83. https://doi.org/10.1007/BF03176149
Johnson, J.G., Klapper, G., Sandberg, C.., 1985. Devonian eustatic fluctuations in Euramerica. Geol Soc Am Bull 96, 567–587. https://doi.org/10.1130/0016-7606(1985)96<567:DEFIE>2.0.CO;2
Johnson, J.G., Murphy, M.A., 1984. Time-rock model for Siluro-Devonian continental shelf, western United States. Geol. Soc. Am. Bull. 95, 1349–1359.
Jones, C.L., 1965. Petrography of evaporites from the Wellington Formation near Hutchinson. Kansas US Geol. Surv. Bull.

Kendall, A.C., 2010. Marine Evaporites, in: Jones, N.P., Dalrymple, R.W. (Eds.), Facies Models. Geological Association of Canada, pp. 505–539.
Kendall, A.C., 1978. Facies models 12. Subaqueous evaporites. Geosci. Canada 5.
Klingspor, A.M., 1969. Middle Devonian Muskeg evaporites of western Canada. Am. Assoc. Pet. Geol. Bull. 53, 927–948.
Koehler, G., Kyser, T.K., Enkin, R., Irving, E., 1997. Paleomagnetic and isotopic evidence for the diagenesis and alteration of evaporites in the Paleozoic Elk Point Basin, Saskatchewan, Canada. Can. J. Earth Sci. 34, 1619–1629. https://doi.org/10.1139/e17-130
Lowenstein, T., 1987. Primary features in a potash evaporite deposit, the Permian Salado Formation of west Texas and New Mexico. Soc. Econ. Paleontol. Mineral. 276–304.
Lowenstein, T.K., 1988. Origin of depositional cycles in a Permian "saline giant": The Salado (McNutt zone) evaporites of New Mexico and Texas. Bull. Geol. Soc. Am. 100, 592–608. https://doi.org/10.1130/0016-7606(1988)100<0592:OODCIA>2.3.CO;2
Lowenstein, T.K., Hardie, L.A., 1985. Criteria for the recognition of salt-pan evaporites. Sedimentology 32, 627–644. https://doi.org/10.1111/j.1365-3091.1985.tb00478.x
Lowenstein, T.K., Hein, M.C., Bobst, A.L., Jordan, T.E., Ku, T.-L., Luo, S., 2003. An Assessment of Stratigraphic Completeness in Climate-Sensitive Closed-Basin Lake Sediments: Salar de Atacama, Chile. J. Sediment. Res. 73, 91–104. https://doi.org/10.1306/061002730091
Lowenstein, T.K., Li, J., Brown, C., Roberts, S.M., Ku, T.-L.L., Luo, S., Yang, W., Li, J., Brown, C., Roberts, S.M., Ku, T.-L.L., Luo, S., Yang, W., 1999. 200 ky paleoclimate record from Death Valley salt core. Geology 27, 3–6. https://doi.org/10.1130/0091-7613(1999)027<0003:KYPRFD>2.3.CO;2
Lowenstein, T.K., Risacher, F., 2009. Closed basin brine evolution and the influence of Ca-Cl inflow waters: Death valley and bristol dry lake California, Qaidam Basin, China, and Salar de Atacama, Chile. Aquat. Geochemistry 15, 71–94. https://doi.org/10.1007/s10498-008-9046-z
Lugli, S., 2009. Evaporites, Encyclopedia of Earth Sciences Series. https://doi.org/10.1007/978-1-4020-4411-3_84
Maiklem, W.R., 1971. Evaporative drawdown - a mechanism forwater-level lowering and diagenesis in the Elk Point Basin. Bull. Can. Pet. Geol. 19, 487–501.
McCabe, W.S., 1954. Williston Basin Paleozoic Unconformities. Am. Assoc. Pet. Geol. Bull. 38, 1997–2010. https://doi.org/10.1306/5ceae05b-16bb-11d7-8645000102c1865d
McTavish, G.J., Vigrass, L.W., 1987. Salt dissolution and tectonics, south-central Saskatchewan. Fifth International Williston Basin Symposium Proceedings.
Meijer Drees, N.C., 1994. Devonian Elk Point Group of the Western Canada Sedimentary Basin., in: Mossop Shetson, I.G.D. (Ed.), Geological Atlas of the Western Canada Sedimentary Basin. Alberta Research Council, Canadian Society of Petroleum Geology, pp. 129–147.
Meijer Drees, N.C., Nowlan, G.S., Fowler, M.., Stasiuk, L.D., McGregor, D.C., Palmer, B.R., Addison, G.., 2002. Lithostratigraphy, sedimentology, paelontology, organic petrology, and organic geochemistry of the Middle Devonian Ashern, Winnipegosis, and Eyot Formations in East-Central Alberta and West-Central Saskatchewan. Geol. Surv. Canada.
Mossman, D.J., Delabio, R.N., Mackintosh, D., 1982. Mineralogy of clay marker seams in some Saskatchewan potash mines. Can. J. Earth Sci. 19, 2126–2140. https://doi.org/10.1139/e82-

187
Powers, D.W., Holt, R.M., 2007. The Salt That Wasn't There: Mudflat Facies Equivalents to Halite of the Permian Rustler Formation, Southeastern New Mexico. J. Sediment. Res. 70, 29–36. https://doi.org/10.1306/2dc408fb-0e47-11d7-8643000102c1865d
Pysklywec, R.N., Mitrovica, J.X., 2000. Mantle flow mechanisms of epeirogeny and their possible role in the evolution of the Western Canada Sedimentary Basin. Can. J. Earth Sci. 37, 1535–1548. https://doi.org/10.1139/e00-057
Robertson, C.H., 1990. Halite depositional facies in a solar salt pond: A key to interpreting physical energy and water depth in ancient deposits? Geology 18, 691–694.
Rogers, M.B., 2017. Stratigraphy of the Middle Devonian Keg River and Prairie Evaporite formations, northeast Alberta, Canada. Bull. Can. Pet. Geol. 65, 5–63. https://doi.org/10.2113/gscpgbull.65.1.5
Schreiber, B.C., Lugli, S., Babel, M., 2007. Evaporites Through Space and Time, Geological Society Special Publications. The Geological Society, London.
Scotese, C.R., 2001. Atlas of Earth History 58. https://doi.org/10.1017/CBO9781107415324.004
Sherwin, D.F., 1962. Lower Elk Point Section in East-Central Alberta. Alberta Soc. if Pet. Geol. 10, 185–191.
Sherwin, D.F., Api, S., 1962. Lower Elk Point section in east-central Alberta. Bull. Can. Pet. Geol. 10, 185–191.
Smoot, J.P., Lowenstein, T.K., 1991. Depositional environments of non-marine evaporites. Dev. Sedimentol. 50, 189–347. https://doi.org/10.1016/S0070-4571(08)70261-9
Spencer, R.J., 1987. Origin of CaCl brines in Devonian formations, western Canada sedimentary basin. Appl. Geochemistry 2, 373–384. https://doi.org/10.1016/0883-2927(87)90022-9
Stein, M., 2001. The sedimentary and geochemical record of neogene-quaternary water bodies in the Dead Sea basin - Inferences for the regional paleoclimatic history. J. Paleolimnol. 26, 271–282. https://doi.org/10.1023/A:1017529228186
Taj, R.J., Aref, M.A., 2015. Structural and textural characteristics of surface halite crusts of a supratidal, ephemeral halite pan, South Jeddah, Red Sea Coast, Saudi Arabia. Facies 61, 2. https://doi.org/10.1007/s10347-014-0426-0
Wardlaw, N.C., Reinson, G.E., 1971. Carbonate and evaporite deposition and diagenesis, Middle Devonian Winnipegosis and Prairie Evaporite formations of south-central Saskatchewan. Am. Assoc. Pet. Geol. Bull. 55, 1759–1786. https://doi.org/10.1306/819A3DA4-16C5-11D7-8645000102C1865D
Wardlaw, N.C., Schwerdtner, W.M., 1966. Halite-anhydrite seasonal layers in the middle Devonian Prairie evaporite formation, Saskatchewan, Canada. Geol. Soc. Am. Bull. 77, 331–342. https://doi.org/10.1130/0016-7606(1966)77[331:HSLITM]2.0.CO;2
Warren, John K, 2016. Interpreting Evaporite Textures BT - Evaporites: A Geological Compendium, in: Warren, J.K. (Ed.), . Springer International Publishing, Cham, pp. 1–83. https://doi.org/10.1007/978-3-319-13512-0_1
Warren, John K., 2016. Sabkhas, Saline Mudflats and Pans, Evaporites. https://doi.org/10.1007/978-3-319-13512-0_3
Wenk, H.-R., Bulakh, A., 2016. Minerals: their constitution and origin. Cambridge University Press.
Williams, G.K., 1984. Some musings on the Devonian Elk Point basin, western Canada. Bull. Can. Pet. Geol. 32, 216–232.

Witzke, B.J., Heckel, P.H., 1988. Paleoclimatic indicators and inferred Devonian paleolatitudes of Euramerica 1, 49–63.
Worsley, N., Fuzesy, A., 1979. The Potash-bearing members of the Devonian Prairie Evaporite of Southeastern Saskatchewan, South of the mining area. Econ. Geol. 74, 377–388.

## Appendix A: Well Data

Names, well ID, location, depth and formation intersection of all wells used in this project are available in the UAL Dataverse dataset at Raw data is available at https://doi.org/10.7939/DVN/LEXODD.

## Appendix B: XRD Data

.

**Table B1** Results of XRD analysis for 33 samples from Wells # 1, #3, and #6, conducted at the University of Alberta. Analysed samples are offcuts of core from Wells #1, #3, and #6.

| Well | Sample ID | Minerals present, as listed in order of decreasing semi-quantitative abundance | Interpreted sample facies |
|---|---|---|---|
| #6 | 1-33 b2 | Calcite, dolomite, halite, quartz, muscovite, anhydrite | Marlstone & anhydritic mud |
| #6 | 1-33 c3 | Kaolinite, dolomite, halite, quartz, muscovite | Sylvinite, fibrous red salt filling fracture |
| #6 | 1-33 d1 | Ankerite, halite, microcline | Sylvinite |
| #6 | 1-33 e2 | Halite, anhydrite | Sylvinite |
| #6 | 1-33 f1 | Halite, anhydrite | Sylvinite |
| #6 | 1-33 g2 | Halite | Bedded halite |
| #6 | 1-33 h2 | Halite, anhydrite | Bedded halite |
| #6 | 1-33 i1 | Halite, anhydrite, dolomite | Bedded halite |
| #1 | 16-33 a6 | Quartz, anhydrite, dolomite, halite, muscovite, sanidine, clinochlore | Marlstone, fibrous red salt filling fracture |
| #1 | 16-33 b1 | Quartz, anhydrite, dolomite, halite | Halite with chaotic mudstone |
| #1 | 16-33 b8 | Quartz, anhydrite, dolomite, halite | Halite with chaotic mudstone |
| #1 | 16-33 c1 | Dolomite, halite | Bedded halite |
| #1 | 16-33 c8 | Dolomite, halite, anhydrite | Halite with chaotic mudstone |
| #1 | 16-33 d1 | Dolomite, halite, anhydrite | Coarse clear halite, bedded halite |
| #1 | 16-33 d9 | Dolomite, halite | Bedded halite |
| #1 | 16-33 e1 | Halite, sulphohalite, anhydrite, dolomite | Coarse clear halite, bedded halite |
| #1 | 16-33 e10 | Halite, anhydrite, dolomite | Bedded halite |
| #1 | 16-33 f1 | Halite, anhydrite, dolomite, sylvite, carnallite | Coarse clear halite, bedded halite |
| #1 | 16-33 f7 | Halite, anhydrite, dolomite | Halite with chaotic mudstone |
| #1 | 16-33 g1 | Dolomite, muscovite, halite, sylvite, microcline, anhydrite | Halite with chaotic mudstone |
| #1 | 16-33 g9 | Halite, anhydrite | Bedded halite |
| #1 | 16-33 g11 | Halite, anhydrite, dolomite, quartz | Halite with chaotic mudstone |
| #1 | 16-33 h2 | Halite, anhydrite | Bedded halite |

| | | | |
|---|---|---|---|
| #1 | 16-33 h10 | Halite, anhydrite, quartz, dolomite | Halite with chaotic mudstone |
| #1 | 16-33 i1 | Halite, anhydrite | Bedded halite |
| #3 | 6-12 32p1 | Halite, anhydrite | Bedded halite |
| #3 | 6-12 35 p2 | Halite, anhydrite, dolomite, quartz | Halite with chaotic mudstone |
| #3 | 6-12 42 | Halite, anhydrite, dolomite, quartz | Halite with chaotic mudstone |
| #3 | 6-12 48 p1 | Halite, anhydrite, dolomite | Bedded halite |
| #3 | 6-12 51 p2 | Halite, anhydrite, dolomite | Bedded halite |
| #3 | 6-12 55p2 | Halite | Bedded halite |
| #3 | 6-12 59 p2 | Halite, anhydrite, dolomite | Bedded halite |
| #3 | 6-12 63p2 | Halite, anhydrite, dolomite | Bedded halite |

# Appendix C: ICP-MS Data

**Table C1** Elemental compositions of 31 samples determined by solution ICP-MS at the University of Alberta. Elemental data are expressed in ppm. * Data available in the UAL repository. Compositions of secondary standard GSP-2 determined during this study are compared with the reference value and reported as % recovery relative to the reference value. -: not available

*<DL:* below lower limit of detection.

| **Analyte** | **B** | **Na** | **Mg** | **Al** | Si | **P** | **K** | **Ca** | **Fe** | **Mn** | **Cu** | **Zn** | **Rb** | **Sr** |
|---|---|---|---|---|---|---|---|---|---|---|---|---|---|---|
| Detection Limits (DL) | 2 | 0.5 | 2 | 0.2 | 5 | 5 | 6 | 31 | 3.7 | 0.03 | 0.03 | 0.08 | 0.04 | 0.03 |
| Units | ppm | ppm | ppm | ppm | ppm | ppm | ppm | ppm | ppm | ppm | ppm | ppm | ppm | ppm |
| 1-33 B2 | <DL | 225286 | 22433 | 13929 | 10836 | 185 | 10307 | 60296 | 9507 | 86.6 | 15.1 | 13.6 | 29.8 | 199 |
| 1-33 C3 | <DL | 307379 | 16295 | 9598 | 1919 | 98 | 6594 | 20141 | 4593 | 52.8 | 14.6 | 7.68 | 21.8 | 48.1 |
| 1-33 D1 | <DL | 382539 | 693 | 348 | <DL | 28 | 5600 | 1988 | 211 | 2.55 | 15.9 | <DL | 1.29 | 9.47 |
| 1-33 E2 | <DL | 395057 | 190 | 32.3 | 19 | 35 | 804 | 2325 | 35.7 | 0.91 | 32.5 | 2.64 | 0.13 | 12.5 |
| 1-33 F1 | <DL | 400869 | 1250 | 734 | <DL | 29 | 815 | 2227 | 375 | 4.03 | 29.9 | 1.51 | 1.45 | 9.52 |
| 1-33 G2 | <DL | 346461 | 375 | 143 | 20 | 26 | 352 | 459 | 237 | 0.82 | 21.0 | <DL | 0.31 | 5.71 |
| 1-33 H2 | <DL | 353742 | 284 | 101 | <DL | 38 | 111 | 2325 | 168 | 0.56 | 18.0 | <DL | 0.16 | 7.32 |
| 1-33 I1 | <DL | 374022 | 775 | 52.8 | <DL | 19 | 78 | 1855 | 185 | 0.97 | 20.0 | <DL | 0.09 | 3.96 |
| 16-33 A6 | 11 | 22028 | 31749 | 20094 | <DL | 311 | 19435 | 125613 | 18933 | 139 | 7.82 | 22.4 | 43.1 | 602 |
| 16-33 B1 | <DL | 335537 | 10126 | 7663 | 201 | 111 | 5689 | 15330 | 4013 | 39.5 | 16.8 | 6.10 | 14.5 | 41.7 |
| 16-33 B8 | <DL | 386740 | 5461 | 2667 | 380 | 54 | 2104 | 7309 | 1249 | 14.5 | 18.3 | 2.34 | 5.20 | 23.9 |
| 16-33 C1 | <DL | 344196 | 1909 | 985 | <DL | 46 | 777 | 2052 | 491 | 5.01 | 15.8 | 0.62 | 1.84 | 12.2 |
| 16-33 C8 | <DL | 360959 | 1691 | 1119 | <DL | 11 | 1023 | 4691 | 531 | 5.22 | 17.4 | 1.45 | 2.04 | 21.3 |
| 16-33 D1 | <DL | 392873 | 274 | 104 | 11 | 12 | 1290 | 931 | 104 | 0.59 | 18.8 | 0.44 | 0.41 | 6.77 |
| 16-33 D9 | <DL | 344591 | 478 | 228 | <DL | 41 | 392 | 966 | 181 | 1.47 | 15.6 | 0.99 | 0.45 | 5.38 |
| 16-33 E1 | <DL | 673 | 1876 | 134 | <DL | 34 | 3355 | 1712 | 160 | 1.27 | 14.9 | 2.06 | 2.42 | 10.1 |
| 16-33 E10 | <DL | 367669 | 619 | 30.7 | <DL | 21 | 541 | 19316 | 104 | 0.39 | 16.3 | 1.22 | 0.26 | 70.7 |

| | | | | | | | | | | | | | | |
|---|---|---|---|---|---|---|---|---|---|---|---|---|---|---|
| 16-33 F1 | <DL | 327798 | 3262 | 44.6 | <DL | 19 | 5134 | 24337 | 80.5 | 0.96 | 16.3 | <DL | 3.77 | 77.7 |
| 16-33 F7 | <DL | 402995 | 3623 | 731 | <DL | 35 | 2005 | 6043 | 419 | 5.05 | 18.8 | <DL | 2.15 | 23.4 |
| 16-33 G1 | <DL | 327057 | 15127 | 5322 | 4929 | 77 | 3394 | 19065 | 2444 | 28.8 | 15.1 | 4.95 | 8.79 | 41.9 |
| 16-33 G11 | <DL | 314753 | 14439 | 7841 | 8037 | 124 | 4793 | 33636 | 3652 | 43.8 | 16.7 | 8.89 | 12.9 | 83.0 |
| 16-33 H2 | <DL | 371486 | 200 | 57.2 | 37 | 46 | 166 | 5365 | 132 | 0.50 | 16.2 | 0.23 | 0.12 | 17.3 |
| 16-33 I1 | <DL | 395461 | 215 | 144 | 16 | 53 | 135 | 1757 | 173 | 0.92 | 17.6 | 2.72 | 0.29 | 7.07 |
| 6-12 32P1 | <DL | 358277 | 1164 | 743 | <DL | 51 | 680 | 3033 | 551 | 4.49 | 19.8 | 1.11 | 1.44 | 17.8 |
| 6-12 35P2 | <DL | 340049 | 10803 | 6257 | 2179 | 81 | 4807 | 15526 | 3064 | 24.3 | 16.1 | 3.20 | 15.4 | 49.3 |
| 6-12 42 | <DL | 368354 | 2148 | 1017 | 49 | 42 | 893 | 11522 | 490 | 4.96 | 17.7 | 0.36 | 1.89 | 41.8 |
| 6-12 48P1 | <DL | 400364 | 745 | 456 | <DL | 42 | 582 | 2163 | 277 | 2.55 | 18.9 | <DL | 0.92 | 9.19 |
| 6-12 51P2 | <DL | 389592 | 450 | 245 | <DL | 31 | 285 | 7394 | 220 | 2.09 | 19.1 | 0.35 | 0.44 | 30.4 |
| 6-12 55P2 | <DL | 329935 | 87 | 40.2 | <DL | 13 | 135 | 263 | 101 | 0.39 | 16.6 | 0.16 | <DL | 2.23 |
| 6-12 59P2 | <DL | 310406 | 292 | 103 | <DL | 30 | 171 | 9873 | 216 | 1.07 | 15.6 | 0.95 | 0.16 | 36.8 |
| 6-12 63P2 | <DL | 370460 | 71 | 39.5 | <DL | 36 | 98 | 1264 | 120 | 0.37 | 18.4 | 0.34 | <DL | 3.46 |
| **Secondary standard analyses** | | | | | | | | | | | | | | |
| Certified value | - | 20600 | 5800 | 78800 | - | 1300 | 44800 | 15000 | 34300 | 320 | 43 | 120 | 245 | 240 |
| GSP-2 (1) | <DL | 21688 | 6065 | 72414 | <DL | 1226 | 45576 | 14592 | 30903 | 319 | 52.5 | 120 | 249 | 238 |
| % recovery | - | 105.3 | 104.6 | 91.9 | - | 94.3 | 101.7 | 97.3 | 90.1 | 99.6 | 122.1 | 100.4 | 101.7 | 99.1 |
| GSP-2 (2) | <DL | 19368 | 5023 | 52222 | <DL | 1130 | 39852 | 11632 | 30007 | 270 | 47.2 | 120 | 194 | 169 |
| % recovery | - | 94.0 | 86.6 | 66.3 | - | 87.0 | 89.0 | 77.5 | 87.5 | 84.4 | 109.7 | 99.7 | 79.0 | 70.2 |

**Table C2** Elemental compositions (including Hg) of 31 samples determined by solution ICP-MS at the University of Alberta. Elemental data are expressed in ppm. * Data available at ual online repository.

| Sample ID | Depth | Rb | Sr | Hg | Pb |
|---|---|---|---|---|---|
| 1-33 B2 | 1402.9 | 34.96 | 246.93 | < DL | 1.53 |
| 1-33 C3 | 1410.58 | 23.08 | 53.2 | < DL | 1.3 |
| 1-33 D1 | 1428.04 | 1.42 | 10.32 | < DL | 0.32 |
| 1-33 E2 | 1435.76 | 0.21 | 13.09 | < DL | 0.15 |
| 1-33 F1 | 1441.18 | 1.44 | 9.77 | < DL | 0.23 |
| 1-33 g2 | 1449 | 0.42 | 5.87 | < DL | 0.12 |
| 1-33 h2 | 1456 | 0.29 | 9.15 | < DL | 0.32 |
| 1-33 i1 | 1464 | 0.21 | 4.39 | < DL | 0.22 |
| 16-33 a6 | 1368.12 | 53.88 | 659.67 | 0.17 | 3.13 |
| 16-33 b1 | 1371.3 | 14.3 | 44.25 | 0.1 | 0.84 |
| 16-33 b8 | 1379.7 | 4.39 | 19.49 | < DL | 0.72 |
| 16-33 c1 | 1386.04 | 2.21 | 13.85 | < DL | 0.3 |
| 16-33 c8 | 1392.87 | 2.03 | 23.08 | < DL | 0.35 |
| 16-33 d1 | 1401 | 0.32 | 4.51 | < DL | 0.14 |
| 16-33 d9 | 1412.01 | 0.61 | 5.97 | < DL | 0.2 |
| 16-33 e1 | 1417.19 | 2.67 | 9.95 | 0.05 | 0.46 |
| 16-33 e10 | 1427.96 | 0.2 | 47.25 | < DL | 0.19 |
| 16-33 f1 | 1432.19 | 3.57 | 80.53 | < DL | 0.27 |
| 16-33 f7 | 1439.5 | 2.02 | 21.61 | < DL | 0.33 |
| 16-33 g1 | 1447.74 | 8.62 | 42.03 | < DL | 0.65 |
| 16-33 g11 | 1459.44 | 13.51 | 77.28 | < DL | 1.68 |
| 16-33 h2 | 1464.13 | 0.21 | 20.41 | < DL | 0.28 |
| 16-33 i1 | 1477.88 | 0.34 | 6.81 | < DL | 0.35 |
| 6-12 32p1 | 3485.2 | 1.37 | 12.11 | < DL | 0.58 |
| 6-12 35 p2 | 3519.2 | 13.95 | 44.84 | < DL | 1.08 |
| 6-12 42 | 3582.1 | 1.83 | 41.27 | < DL | 1.45 |
| 6-12 48 p1 | 3756.1 | 0.97 | 9.42 | < DL | 0.37 |
| 6-12 51 p2 | 3789.6 | 0.47 | 32.57 | < DL | 0.41 |
| 6-12 55p2 | 3829.3 | 0.17 | 3.66 | < DL | 0.5 |
| 6-12 59 p2 | 3853.9 | 0.29 | 41.57 | < DL | 1.36 |
| 6-12 63p2 | 3907.3 | 0.14 | 4.86 | < DL | 0.73 |

## Appendix D: MicroCT porosity Data

MicroCT scans for 27 samples were conducted at the University of Alberta to assess sample porosity. Porosity is given in terms of percent of volume (Vol %).

**Table D1** MicroCT porosity analysis results for core from Well #3

| Sample name | Porosity (%) |
|---|---|
| 32P1 | 1.85 |
| 35P2 | 6.99 |
| 42 | 15.81 |
| 48P1 | 14.33 |
| 51P2 | 0.71 |
| 55P2 | 1.67 |
| 63P2 | 2.49 |

**Table D2** MicroCT porosity analysis results for core from Well #6

| Sample name | Porosity (%) |
|---|---|
| 32P1 | 1.85 |
| 35P2 | 6.99 |
| 42 | 15.81 |
| 48P1 | 14.33 |
| 51P2 | 0.71 |
| 55P2 | 1.67 |
| 63P2 | 2.49 |

**Table D3** MicroCT porosity analysis results for core from Well #1

| Sample name | Porosity (%) |
|---|---|
| B1 | -2.08 |
| B8 | 0.86541 |
| C1 | 0.909717 |
| C8 | 3.448592 |
| D1 | 2.080513 |
| D9 | 2.962563 |
| E1 | 3.79017 |
| F1 | 8.041288 |
| F7 | 2.813402 |
| 2 | 5.561451 |
| I1 | -1.5516 |
| G11 | 7.617321 |
| E10 | 4.167058 |

# Plates


**Plate 1** Bedded halite in core from well #3.

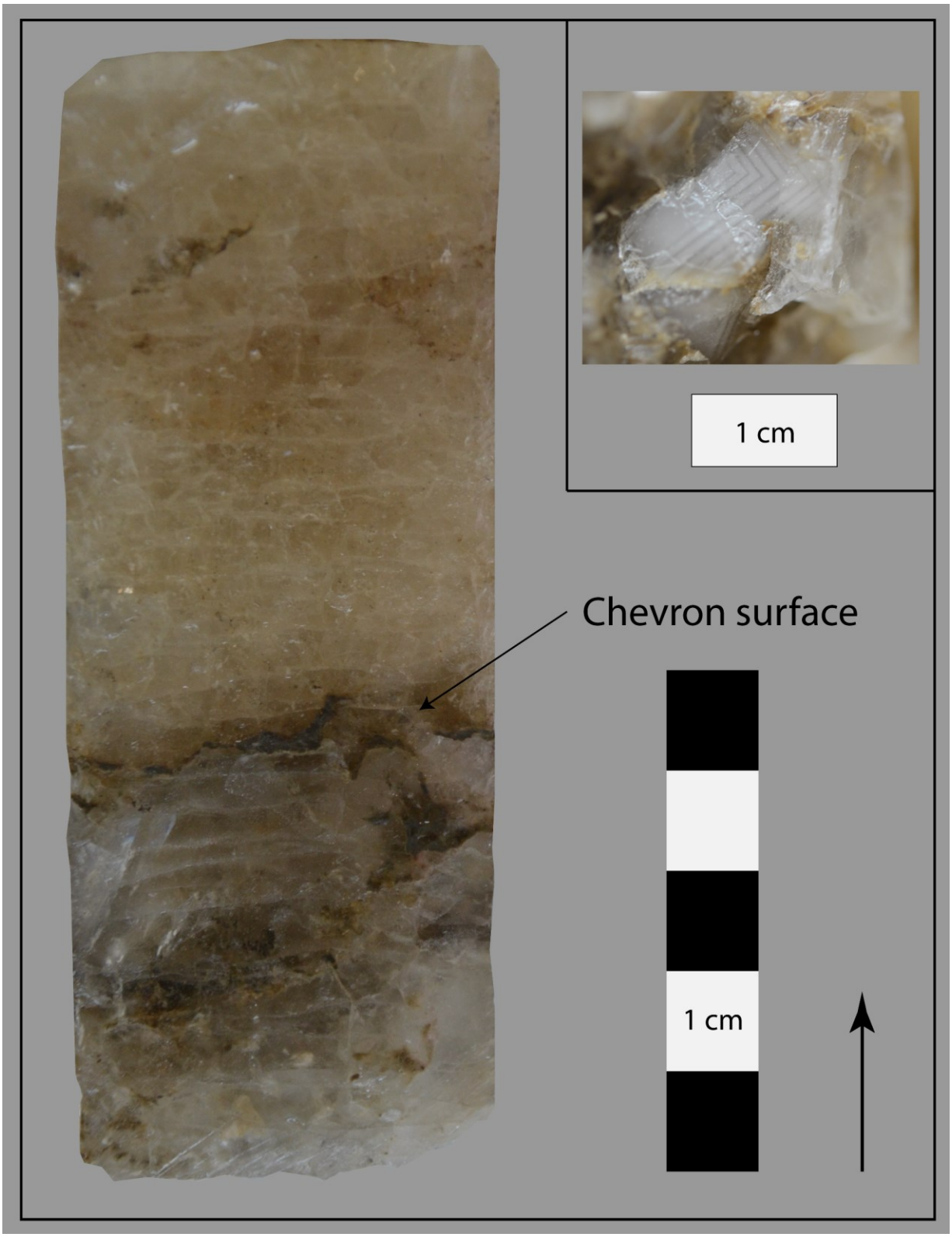


**Plate 2** Chevron crystal growth in core from well #3.


**Plate 3** Mud draping in core from well #3.

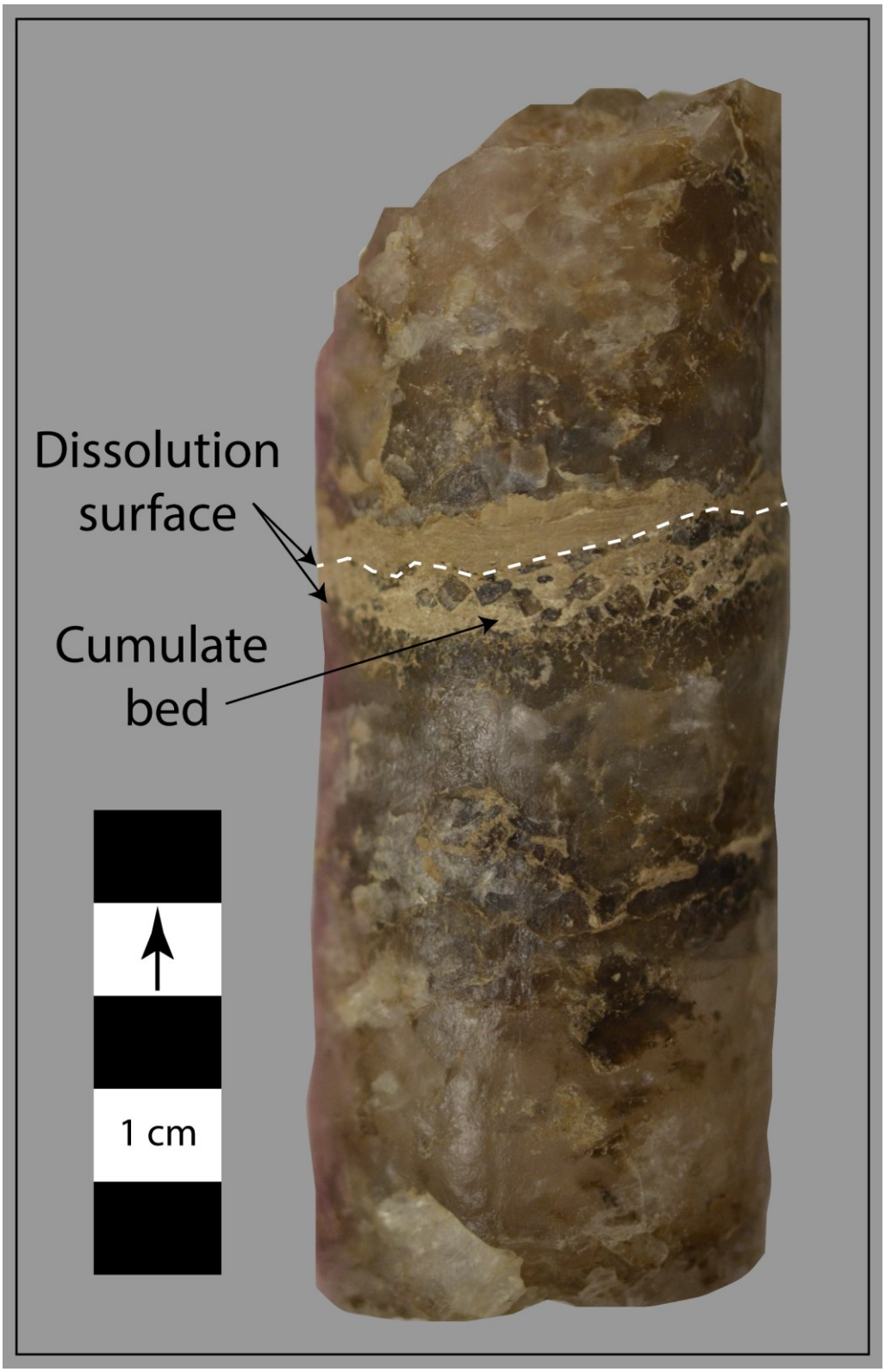


**Plate 4** Cumulate bed and dissolution surface in core from well #3.

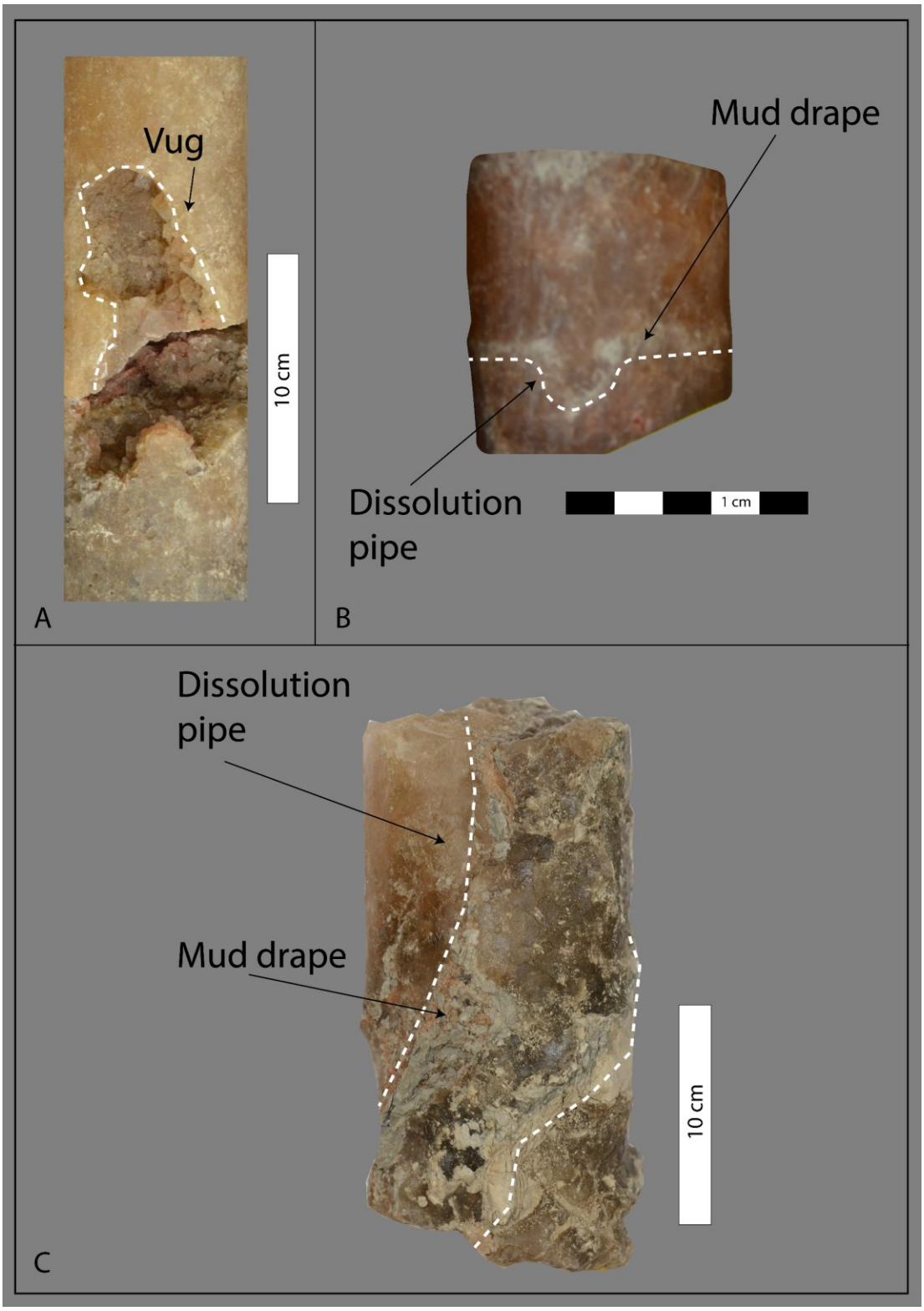


**Plate 5** Dissolution features in core from well #3.


**Plate 6** Chaotic mud and halite turbation in core from well #3.

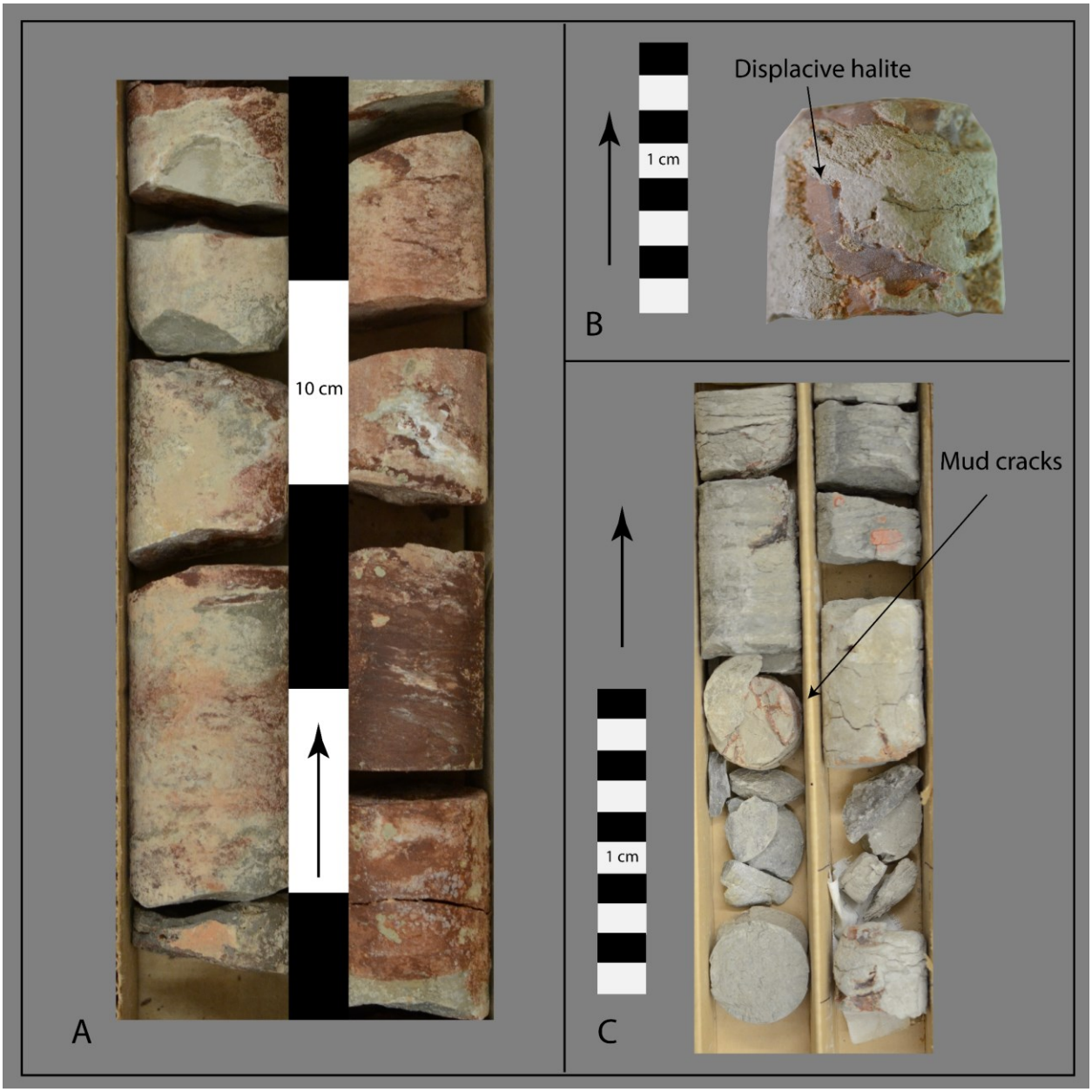


**Plate 7** Exposure surfaces in core from well #3.


**Plate 8** Fibrous red salt filling fractures in core from well #3.

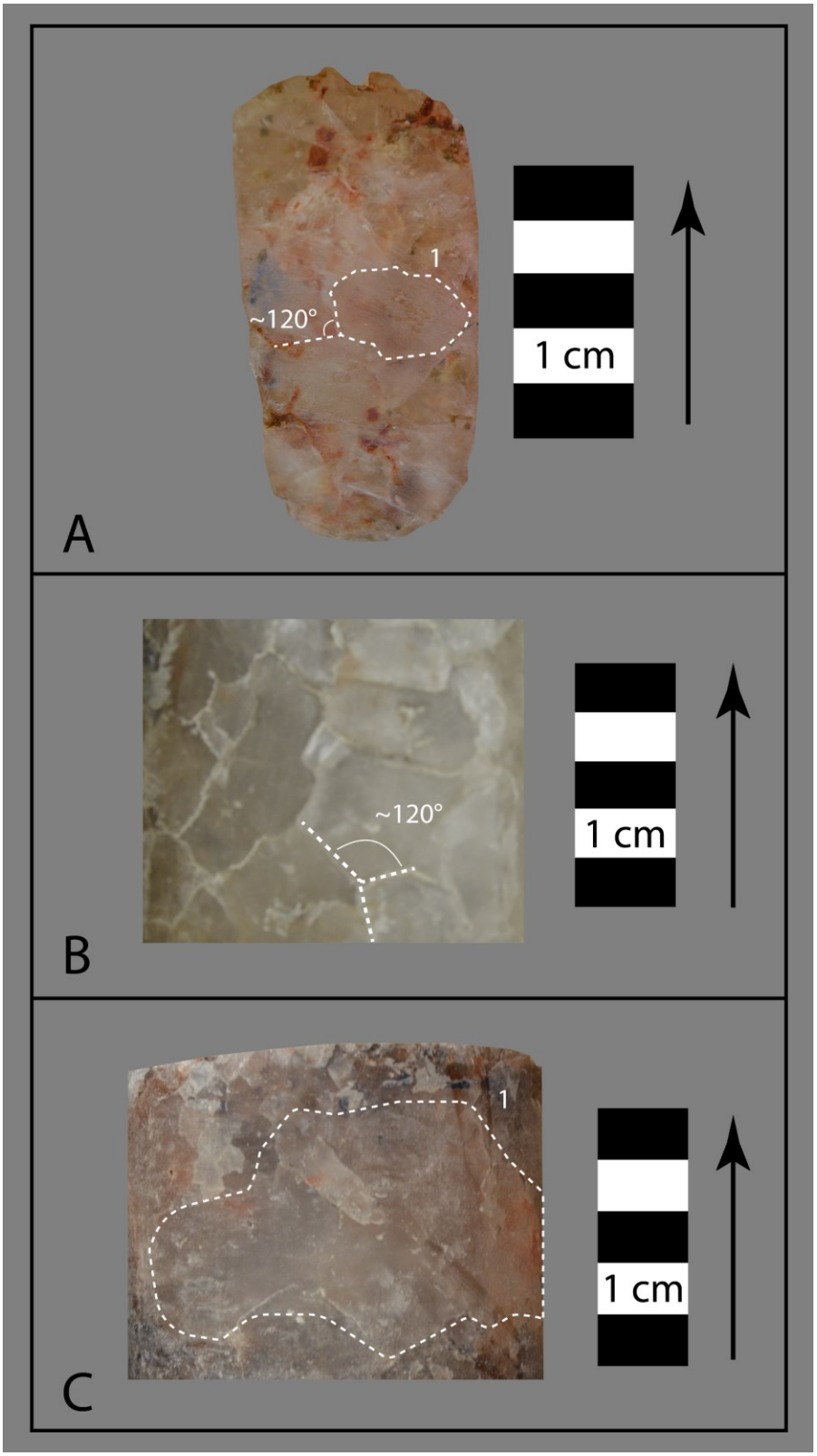


**Plate 9** Diagenetic alteration in halite in core from well #3. A1 – Oblate crystal; C1 – Clear coarse halite >3 cm.